Integrated benchmark simulation model of an immersed membrane bioreactor

Tomasz Janus*, Bogumil Ulanicki

Water Software Systems, De Montfort University, The Gateway, LE1 9BH Leicester, United Kingdom

Abstract

This paper presents a new integrated model of an immersed membrane bioreactor (iMBR) for wastewater treatment. The model is constructed out of three previously published submodels describing the bioreactor, the membrane, and the interface between them. The bioreactor submodel extends a conventional activated sludge model with soluble and bound biopolymers which have been found to cause irreversible and reversible fouling. The membrane model describes fouling as a function of biopolymer concentrations, permeate flow, and shear stresses on the membrane surface. The interface describes the dependency of oxygen transfer rate on suspended solids concentrations and calculates shear stresses on the membrane surface from air-scour rates. The paper serves three purposes. First, the integrated model is simulated on a plant layout of a previously published MBR benchmark model which did not consider any interactions between the submodels. Hence, this paper presents a new and upgraded MBR benchmark model. Secondly, the simulation results showcase how simulations with an integrated model can be used to optimise plant performance and minimise energy consumption. Finally, the paper introduces new measures of

*Corresponding author, Tel.: +44(0) 116 257 7070

Email addresses: tjanus@dmu.ac.uk (Tomasz Janus), bul@dmu.ac.uk (Bogumil Ulanicki)

fouling which can be used for benchmarking different MBR plant layouts and control strategies.

Keywords: benchmark model, biopolymers, EPS, fouling, MBR, SMP

Nomenclature

$AE_{bioreactor}$	energy demand for fine-bubble aeration (kWh d^{-1})
$AE_{membrane}$	energy demand for coarse-bubble aeration (kWh d^{-1})
AE_{total}	total energy demand for aeration (kWh d^{-1})
A_{mem}	total membrane area (m^2)
$BOD_{5,95}$	95%-ile of effluent biological oxygen demand (gO_2 m^{-3})
COD_{95}	95%-ile of effluent chemical oxygen demand (gO_2 m^{-3})
E.Q.	effluent quality index (kgPU d^{-1}) - see Copp (2002) for definition
FI_i	Irreversible fouling index (m^{-1} L^{-1})
FI_r	Reversible fouling index (m^{-1} L^{-1})
$f_{EPS,dh}$	fraction of X_{EPS} produced during heterotrophic biomass decay (gO_2 gO_2^{-1})
$f_{EPS,h}$	fraction of X_{EPS} produced during heterotrophic biomass growth (gO_2 gO_2^{-1})
f_{EPS}^{inf}	extracellular polymeric substances (EPS) content in the influent biomass (–)
f_{nr}	fraction of S_{UAP} and S_{BAP} in the permeate (–)
f_{SMP}^{inf}	S_{BAP} content in the influent S_I (–)
g	gravity constant (9.81 m s^{-2})
h_g	geometric head difference (m H_2O)
h_l	head loss due to friction (m H_2O)
i_{XB}^{inf}	N content of the influent biomass (–)
i_{XEPS}^{inf}	EPS content in the influent biomass (–)
i_{XBAP}^{inf}	N content in BAP (–)
I.Q.	influent quality index (kgPU d^{-1}) - see Copp (2002) for definition
J	permeate flux (L m^{-2} h^{-1})
K_p	proportional gain (varies)
k_i	irreversible fouling strength (m kg^{-1})
k_r	cake detachment constant (kg m^{-2} s^{-1})
ME	energy for mixing anoxic tanks and aerobic tanks in case the amount of air provided is not sufficient for a thorough mixing of the tank contents (kWh d^{-1})
m_i	mass of irreversible foulant per membrane area (kg m^{-2})
m_r	mass of reversible foulant per membrane area (kg m^{-2})

$\dot{m}_r^{back}$	back-flux of reversible foulant per membrane area away from the membrane (kg m^{-2} d^{-1})
OCI	operational cost index (–)
q_a	airflow rate (m^3 d^{-1})
q_{ave}	average flow rate (m^3 d^{-1})
$q_{a,1}$	airflow rate into the first aerobic tank (m^3 d^{-1})
$q_{a,2}$	airflow rate into the second aerobic tank (m^3 d^{-1})
$q_{a,3}$	airflow rate into the membrane tank (m^3 d^{-1})
q_b	backflush flow (m^3 d^{-1})
q_{eff}	effluent (permeate) flow rate (m^3 d^{-1})
q_{inf}	influent flow rate (m^3 d^{-1})
q_{ir}	internal recirculation flow rate (m^3 d^{-1})
q_{ave}	average flow rate (m^3 d^{-1})
q_{min}	minimum flow rate (m^3 d^{-1})
q_{max}	maximum flow rate (m^3 d^{-1})
q_{rec}	sludge recirculation flow rate (m^3 d^{-1})
q_w	waste activated sludge flow rate (m^3 d^{-1})
$\mathrm{PE_{permeate}}$	energy associated with permeate pumping (kWh d^{-1})
$\mathrm{PE}_{q_{back}}$	energy associated with back-flushing (kWh d^{-1})
$\mathrm{PE}_{q_{eff}}$	energy associated with effluent pumping (kWh d^{-1})
$\mathrm{PE}_{q_{int}}$	energy used on internal recirculation (kWh d^{-1})
PE_{q_r}	energy used on sludge recirculation (kWh d^{-1})
PE_{q_w}	energy used on WAS pumping (kWh d^{-1})
$\mathrm{PE_{sludge}}$	energy associated with sludge pumping (kWh d^{-1})
$\mathrm{PE_{total}}$	total pumping energy (kWh d^{-1})
R_i	resistance due to irreversible fouling (m^{-1})
R_m	clean membrane resistance (m^{-1})
R_r	resistance due to reversible fouling (m^{-1})
R_t	total membrane resistance (m^{-1})

S_{ALK}	alkalinity (molHCO$_3^-$ m^{-3})
S_{BAP}	concentration of biomass associated products (BAP) (gO$_2$ m^{-3})
S_{ND}	concentration of soluble organic nitrogen (gN m^{-3})
S_{NH}	concentration of ammoniacal nitrogen (gN m^{-3})
$S_{NH,95}$	95%-ile of effluent ammoniacal nitrogen concentration (gN m^{-3})
S_{NO}	concentration of nitrites and nitrates (gN m^{-3})
S_I	concentration of soluble inert organic matter (gO$_2$ m^{-3})
S_O	dissolved oxygen concentration (gO$_2$ m^{-3})
$\mathrm{SP_{disp}}$	amount of sludge for disposal (kgTSS d^{-1})
$\mathrm{SP_{tot}}$	total sludge production (kgTSS d^{-1})
S_S	concentration of readily biodegradable substrate (gO$_2$ m^{-3})
S_{SMP}	concentration of soluble microbial products (gO$_2$ m^{-3}). $S_{SMP} = S_{UAP} + S_{BAP}$
S_{UAP}	concentration of utilisation associated products (UAP) (gO$_2$ m^{-3})
t_f	filtration cycle duration time (s)
t_I	integral time (d)
T_l	liquid temperature (^{o}C)
$\mathrm{TN_{95}}$	95%-ile of effluent total nitrogen concentration (gN m^{-3})
t_{simu}	simulation time (d)
$\mathrm{TSS_{95}}$	95%-ile of effluent total suspended solids concentration (gN m^{-3})
t_0	simulation start time (d)
v_{sg}	superficial gas velocity (cm s^{-1})
v_{sl}	superficial liquid velocity (cm s^{-1})
$V_{ax,1}$	first anoxic tank volume (m^3)
$V_{ax,2}$	second anoxic tank volume (m^3)
V_{mem}	membrane tank volume (m^3)
V_{eff}^{net}	net volume of permeate discharged from the plant (m^3)
$V_{ox,1}$	first aerobic tank volume (m^3)
$V_{ox,2}$	second aerobic tank volume (m^3)
X_A	concentration of autotrophic biomass (gO$_2$ m^{-3})

X_{EPS}	concentration of extracellular polymeric substances (EPS) (gO_2 m^{-3})
X_I	concentration of particulate inert organic matter (gO_2 m^{-3})
X_H	concentration of heterotrophic biomass (gO_2 m^{-3})
X_{MLSS}	concentration of mixed liquor suspended solids (MLSS) (g m^{-3})
X_{ND}	concentration of particulate organic nitrogen (gN m^{-3})
X_P	concentration of particulate products from biomass decay (gO_2 m^{-3})
X_S	concentration of slowly biodegradable organic substrate (gO_2 m^{-3})
X_{TSS}	concentration of total suspended solids (g m^{-3})
Y_{obs}	observed sludge yield (kgSS kg^1BOD_5)
Y_{SMP}	yield coefficient for heterotrophic growth on S_{UAP} and S_{BAP} (–)
α	oxygen transfer coefficient (–)
α_c	specific cake resistance under field conditions (m kg^{-1})
$\alpha_{c,0}$	specific cake resistance at atmospheric pressure (m kg^{-1})
η	pumping efficiency (–)
μ_{BAP}	maximum specific heterotrophic growth rate on S_{BAP} (d^{-1})
ω	proportionality coefficient in the oxygen transfer coefficient equation ($kg^{-1}TSS$)
ρ_w	density of water (kg m^{-3})
τ_w	average shear stress on the fibre surface (Pa)

Abbreviations

ASM	activated sludge model
ASM1	Activated Sludge Model No. 1
ASP	activated sludge process
BAP	biomass associated products
BSM1	COST/IWA benchmark simulation model No.1
BSM-MBR	membrane bioreactor (MBR) benchmark simulation model
C	carbon
CASP	conventional activated sludge process
CES-ASM1	combined EPS and SMP production ASM1-based model
CFD	Computational Fluid Dynamics
COD	chemical oxygen demand
DO	dissolved oxygen
DWF	dry weather flow
EPS	extracellular polymeric substances
FSD	floc size distribution
HF	hollow fibre
IBMF-MBR	integrated bioreactor and membrane fouling MBR model
MBR	membrane bioreactor
MLSS	mixed liquor suspended solids
MWD	molecular weight distribution
N	nitrogen
NF	nanofiltration
NH_4^+-N	ammoniacal nitrogen
NO_3^--N	nitrate nitrogen
P	phosphorus
PI	proportional integral
P&ID	piping and instrumentation diagram
PAC	powdered activated carbon
RAS	recirculated activated sludge

RO	reverse osmosis
SAD_m	specific aeration demand per membrane area
SMP	soluble microbial products
SRT	sludge retention time
TMP	trans-membrane pressure
TKN	total Kjeldahl nitrogen
TN	total nitrogen
UAP	utilisation associated products
UF	ultrafiltration
WAS	waste activated sludge
WWTP	wastewater treatment plant

1. Introduction

MBR systems are widely applied in municipal and industrial wastewater treatment. The main three reasons for their popularity are: tightening effluent discharge standards, rising water scarcity, and limited land availability for expansion of existing wastewater treatment plants (WWTPs). Under such circumstances membrane bioreactors (MBRs) outperform traditional treatment systems thanks to superior effluent quality, better process stability and smaller footprint. The effluent is partly disinfected and can be reused for non-drinking purposes or used as feed for further treatment processes for recycling and water conservation. Despite of a widespread use of MBRs in wastewater treatment the technology is currently missing bespoke dynamic process models that would allow simulation of MBR-based plants in commercial WWTP simulation packages along with conventional processes such as activated sludge reactors, trickling filters, or sedimentation tanks. None of the commercial packages contain a MBR model which is able to predict bulk liquid concentrations of the most dominant biofoulants, i.e. soluble microbial products (SMP) and extracellular polymeric substances (EPS) despite the fact that SMP and EPS are indispensable for integration of the biological and filtration models as these substances have been found to have a direct impact on the rates of different membrane fouling mechanisms such as pore constriction, pore blocking, and cake filtration (Hoa et al., 2003; Broeckmann et al., 2006; Nuengjamnong, 2006; Wang et al., 2009). Additionally, MBR models in commercial software packages do not provide a detailed mechanistic description of membrane fouling and fouling control mechanisms. As long as the mathematical models for MBR systems do not become richer and the main interactions between the bioreactor and the membrane are not described, tasks such as simulation-based process design, process and energy optimisation, diagnosis, risk-analysis, or control strategy development, which can be carried out using commercial simulation packages on conventional treatment processes such as activated sludge process or anaerobic digestion, will not be able to be performed on MBR systems.

Luckily, recent years have seen a number of dynamic mathematical models of membrane bioreactors described in the scientific literature. These publications are briefly summarised in Janus and Ulanicki (2014, 2015c). Although the MBR model described in this paper has some similarities with these earlier published works, it is also significantly different. The biological model used in this study is set to predict the concentrations of soluble and bound polymers contrary to the majority of biological models developed in the earlier studies which only consider soluble biopolymer kinetics - see Janus and Ulanicki (2015c). It was also ascertained that the biological model obeys mass and charge balance equations which were violated in the activated sludge model of Lu et al. (2001) - the biological model of choice in the studies of Zarragoitia-González et al. (2008) and Di Bella et al. (2008). As shall be seen later in this paper, our biological model additionally produces similar outputs to the widely accepted Activated Sludge Model No. 1 (ASM1), hence allowing easy comparison of results with BSM1 (Copp, 2002) and BSM-MBR (Maere et al., 2011) benchmark models. The fouling model has a simple structure and a small number of parameters which are easy to identify with a 'pen and ruler' approach using flux and pressure data from flux stepping experiments - see Janus and Ulanicki (2015b). Our MBR model also considers the role of both soluble and insoluble biopolymers on reversible and irreversible fouling, contrary to the previously published models which generally only consider the role of SMP in cake filtration (reversible fouling) rather than pore constriction (irreversible fouling), whilst neglecting the effects of EPS on fouling in general. In our model irreversible fouling is assumed to be caused by SMP whilst reversible fouling is accelerated by EPS content in mixed liquor suspended solids (MLSS) which leads to an increase in the specific cake resistance. The cake detachment rate is calculated as a function of air-scour intensity with a formula obtained from the results of a steady-state slug flow model of Zaisha and Dukler (1993) solved on the hollow fibre (HF) membrane module geometry of Busch et al. (2007). These additional interactions between the bioreactor and the membrane described in our integrated MBR model will allow a better process integration and more realistic simulation results, thus increasing our ability to optimise the process, energy, and develop better control strategies. Some of the results from this model have already been, albeit briefly, described in an earlier conference publication of Janus and Ulanicki (2014). The purpose of this earlier publication was to briefly outline the benefits of model integration while the current paper describes in detail the simulation results of the benchmark model and compares these results with the earlier simulation benchmark models of Copp (2002) and Maere et al. (2011).

This paper starts with a formulation of modelling hypotheses and then proposes a model structure built around them. Next, this integrated model is simulated on a plant layout of the MBR benchmark simulation model (BSM-MBR) by Maere et al. (2011), albeit, as shall be described later, with minor changes to the tank volumes. Simulations are performed with inputs and simulation scenarios defined in Copp (2002) and later adopted in Maere et al. (2011). Hence, this paper presents a new MBR benchmark simulation model which extends the BSM-MBR with biopolymer kinetics and fouling. It shall be later referred to as integrated bioreactor and membrane fouling MBR model (IBMF-MBR) as it integrates the biological process with membrane fouling by providing mechanisms of bi-directional interaction between these two parts of an MBR. In order to show the similarities and the differences between both benchmarks the simulation results obtained from IBMF-MBR and BSM-MBR are compared and presented in a tabular form adhering to the convention adopted in Copp (2002) and Maere et al. (2011). To quantify and compare the level of fouling accumulated over the simulation period of each benchmark scenario the paper also introduces a new measure of fouling which is applied separately to irreversible and reversible fouling. The irreversible fouling index FI_i describes the amount of irreversible resistance, R_i, accumulated in the last 7 days of dynamic simulation divided by the net volume of permeate discharged from the plant V_{eff}^{net}, i.e. the volume of permeate produced minus the volume of permeate used for backflushing. The reversible fouling index FI_r describes the average amount of reversible resistance R_r accumulated in one filtration cycle over the last 7 days of dynamic simulation divided by V_{eff}^{net}. Both fouling indices can be used as yet another parameter for the comparison of operating strategies in a benchmark model as well as for the calculation of operational expenditures (OPEX) associated with fouling mitigation. Finally, by demonstrating the outputs of the integrated benchmark model under various control strategies, the paper presents how the model can be used to optimise the process and minimise the energy consumption.

2. Modelling hypotheses and model structure

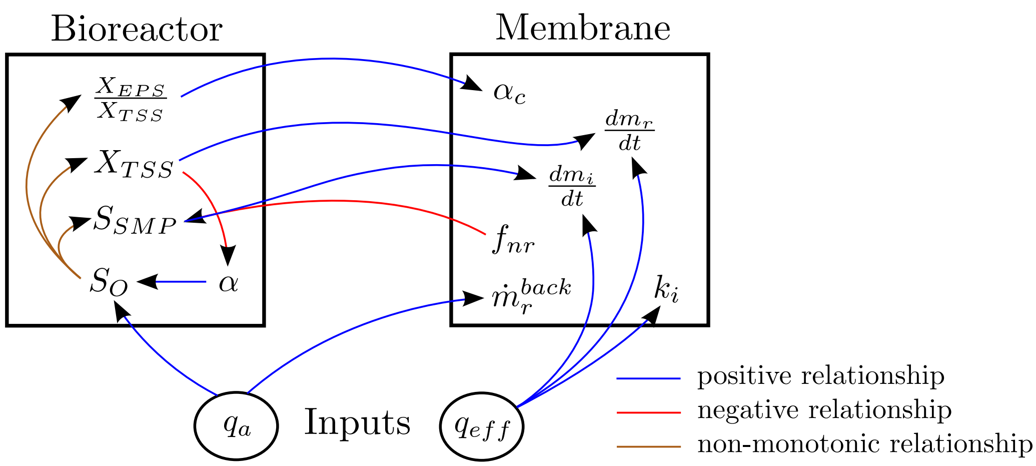

Figure 1: Graphical representation of the links existing between the biological and the filtration part of the IBMF-MBR model.

As earlier explained in Janus and Ulanicki (2015c) the bioreactor is modelled with the combined EPS and SMP production ASM1-based model (CES-ASM1) while the membrane is described with a behavioural fouling model based on the modelling concept of Liang et al. (2006) who divided fouling into two processes based on their intrinsic time constants and reversibility. These two processes, namely irreversible and reversible fouling collectively contribute to the loss of membrane permeability over time. As CES-ASM1 is similar in structure to ASM1 which forms the backbone of BSM1 and BSM-MBR, it is easy to compare the simulation results from IBMF-MBR with the results from the two above earlier simulation benchmark models. Behavioural fouling model was chosen over other more complicated fouling models available in the literature for its simplicity and ease of calibration. Both parts of the system and the links between them are graphically presented in Figure 1. A detailed description of CES-ASM1 and the fouling model can be found in Janus and Ulanicki (2015a) and Janus and Ulanicki (2015b) respectively.

CES-ASM1 predicts the concentrations of various constituents of activated sludge, including bound biopolymers EPS and soluble biopolymers SMP. The EPS fraction in activated sludge $\left(\frac{X_{EPS}}{X_{TSS}}\right)$ determines the value of specific cake resistance α_c according to the modified model of Ahmed et al. (2007). Total solids concentration (X_{TSS}) affects the reversible fouling rate $\left(\frac{dm_r}{dt}\right)$ whilst SMP in the bulk liquid affects the rate of irreversible fouling $\left(\frac{dm_i}{dt}\right)$. SMP concentration in the bioreactor (S_{SMP}) depends on SMP production and utilisation kinetics in the bioreactor as well as the retentive properties of the membrane. Membrane retention is modelled here with parameter f_{nr} representing the fraction of SMP ending up in the permeate.

The rate of cake back-transport from membrane surface depends on coarse-bubble aeration rate q_a. The air bubbles which move upward in the vicinity of the membrane create shear stresses τ_w on the membrane surface leading to detachment of deposited solid particles and preventing new particles to come into contact with the membrane. The relationship between q_a and τ_w is represented with a quadratic polynomial obtained through nonlinear regression on the data points obtained from a solution of a two-phase slug flow model (Janus and Ulanicki, 2015c). The shear stresses are linked to the cake detachment constant k_r accordingly to the model of Nagaoka et al. (1998). Moreover, coarse bubble aeration leads to an increase in oxygen concentration (S_O) in the membrane tank as a result of mass transfer of oxygen from air bubbles to the bulk liquid. The oxygen mass transfer coefficient α is hindered by suspended solids and is described with an empirical relationship $\alpha = e^{-\omega X_{TSS}}$ in which α decreases exponentially with X_{TSS}.

The rates of reversible $\left(\frac{dm_r}{dt}\right)$ and irreversible $\left(\frac{dm_i}{dt}\right)$ fouling depend on the permeate flux J and hence the permeate flow rate q_{eff}. Whilst $\frac{dm_r}{dt} \propto q_{eff}$, $\frac{dm_i}{dt}$ is in a non-linear relationship with q_{eff} because the proportionality constant k_i in the irreversible fouling equation is itself dependent on permeate flux J and hence the permeate flow rate (Janus and Ulanicki, 2015b). The form of this equation, particularly its nonlinearity with respect to flux and linearity with respect to S_{SMP}, has a direct impact on the final simulation results with the IBMF-MBR model which, as shall be explained later, show that irreversible fouling is more sensitive to flux than to bulk liquid SMP concentrations. The membrane is assumed to be 'backflushable', hence the operation of the membrane is assumed to be comprised of filtration and backflush cycles, whilst idle/relaxation cycles are not modelled. The block diagram of the MBR model structure showing the links between the three separate interacting subsystems, i.e. the Bioreactor (Subsystem 1), the Membrane (Subsystem 2) and the Interface (Subsystem 3) can be found in Janus and Ulanicki (2015c) or an earlier publication of Janus and Ulanicki (2014).

3. Plant model description

3.1. Process and instrumentation diagram

The plant layout, simulation scenarios, inputs and control schemes used in the simulations are based on the BSM-MBR simulation benchmark of Maere et al. (2011). However, compared to BSM-MBR, the airflow rates, sludge wastage rates and tank volumes in IBMF-MBR were altered in order to take into consideration the differences in ASM1 and CES-ASM1 model kinetics. The individual reactor volumes are respectively $1,800$ m^3 for anoxic tanks $V_{ax,1}$ and $V_{ax,2}$ and $1,300$ m^3 for aerobic tanks $V_{ox,1}$, $V_{ox,2}$ and the membrane tank V_{mem}. Recirculation, sludge wastage and airflow rates in open-loop simulations and controller setpoints and gains in closed-loop scenarios are provided further down in Section 3.2. The IBMF-MBR simulation model also features a new nitrate control loop, as shown in the piping and instrumentation diagram (P&ID) in Figure 2.

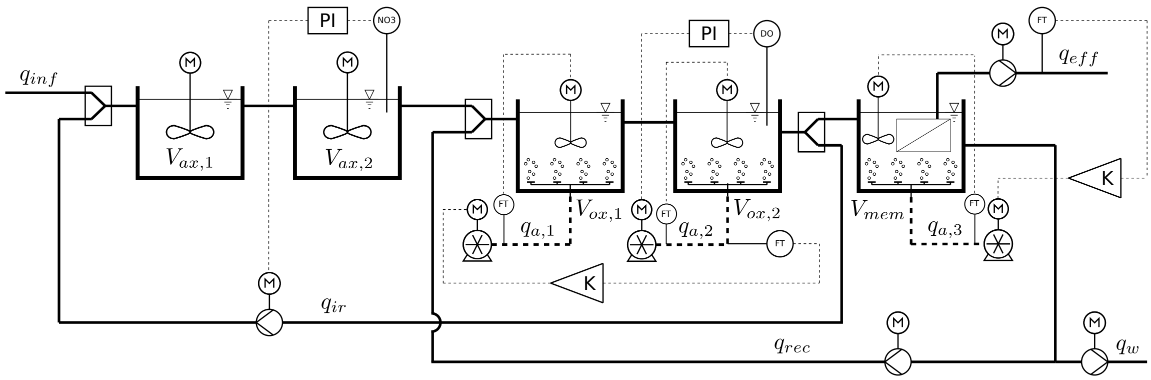

Figure 2: Process and instrumentation diagram of the IBMF-MBR simulation benchmark scheme.

Air supply to the first aerobic tank, the second aerobic tank and the membrane tank is facilitated by three separate air blowers. Mixing of anoxic tanks is carried out with mechanical mixers operating constantly with an assumed energy input of 0.008 kW m^{-3}. Both aerobic tanks and the membrane tank are assumed to be fully mixed if the aeration rate per m^2 of ground surface area in each tank is higher than 2.2 Nm^3 h^{-1} m^{-2}. In times when the actual unit aeration rate in the tank is lower than 2.2 Nm^3 h^{-1} m^{-2}, the tank is assumed to be instead mixed mechanically with the same unit energy demand as the anoxic tanks.

IBMF-MBR simulations are carried out in the same way as described in Copp (2002), i.e. initially under constant flow-averaged inputs for a period of, in our case, 300 days which was found sufficient to reach steady-state for all states in the system, then under time-varying inputs with three different 14-day weather scenarios: dry weather, rain event, and storm event. Each simulation sequence, i.e. steady-state→dry weather→dry weather, steady-state→dry weather→rain event, and steady-state→dry weather→storm event is performed at four levels of process control: (a) open-loop, (b) closed-loop with dissolved oxygen (DO) control, (c) closed-loop with DO and nitrate nitrogen (NO_3^--N) control, and (d) closed-loop with DO, NO_3^--N and specific aeration demand per membrane area (SAD_m) control. All simulations have been performed in SIMBA® v.5.0 software running on MATLAB® R2010.

The three closed-loop control strategies described above are not meant to indicate the most adequate strategies for this particular system, but serve the purpose of demonstrating how different control strategies can be compared using benchmark models such as BSM-MBR or IBMF-MBR. The IBMF-MBR benchmark model developed here adopts the same control strategies as BSM-MBR in order to demonstrate the similarities and the differences between both models under different operating conditions. In all simulations it is assumed that all actuators and sensors are ideal, i.e. without any noise and delay.

3.2. Process control scenarios

In all four process control variants the return activated sludge flow rate, q_{rec}, is set to a constant value of $55,338$ m^3 d^{-1} which is equivalent to 3 times the rate of dry weather flow (DWF). Sludge wastage rate, q_w, is assigned a constant value of 160 m^3 d^{-1} which guarantees a steady-state MLSS concentration in the membrane tank of $\sim$ 10 kg m^{-3}. q_w in IBMF-MBR is lower from the 200 m^3 d^{-1} setpoint used in BSM-MBR due to alteration of the flow of organic substrates in CES-ASM1 as a side-effect of addition of biopolymer kinetics. This resulted in $\sim$ 18.5% lower predicted sludge yields in CES-ASM1 compared to ASM1 as shall be later explained in Sections 5.1 and 5.2.

In the open-loop simulation, internal recirculation, q_{ir}, is kept at a constant rate of $55,338$ m^3 d^{-1} equal to the return activated sludge flow rate q_{rec}. Fine-bubble aeration flow rates, $q_{a,1}$, and $q_{a,2}$, are maintained at $3,440$ Nm^3 d^{-1} and $3,360$ Nm^3 d^{-1} respectively. Total fine bubble aeration flow rate is thus equal to $6,800$ Nm^3 d^{-1}, which is 300 Nm^3 d^{-1} higher than in the BSM-MBR benchmark model. Although the difference in total airflow is minimal, the flow split between both aeration tanks is very different. Whilst the airflow in BSM-MBR was split between $V_{ox,1}$ and $V_{ox,2}$ at 1.89 : 1 ratio, the flow split in CES-ASM1 is near 1 : 1 in open-loop simulations and has been assigned a value of 1.3 : 1 in closed-loop simulations with DO control. Coarse-bubble aeration flow rate, $q_{a,3}$, is kept at $20,025$ Nm^3 d^{-1} which corresponds to SAD_m of 0.3 Nm^3 h^{-1} m^{-2} based on the total membrane area, A_{mem}, of $66,750$ m^2. A_{mem} in BSM-MBR is slightly smaller than $71,500$ m^2 used in Maere et al. (2011) due to reduction of the membrane tank volume, V_{mem}, from $1,500$ m^3 to $1,300$ m^3.

In the closed-loop simulation scenario with DO control DO concentration in the second aerobic tank is kept at 1.5 mgO_2 L^{-1} by a proportional integral (PI) controller set to adjust $q_{a,2}$ based on the signal received from the DO probe positioned in the same tank. $q_{a,1}$ is adjusted in proportion to $q_{a,2}$ at a 1.3 : 1 ratio. The PI controller has been assigned the same gains as in the BSM-MBR benchmark model of Maere et al. (2011), i.e. $K_p = 500$ Nm^3 h^{-1} per mgO_2 L^{-1} and $t_I = 0.002$ d.

In the closed-loop simulation scenario with DO and nitrate control, denitrification is additionally controlled via a PI controller which is set to keep the nitrate concentration in the second anoxic tank at a constant setpoint of 1.0 $mgNO_3^-$ L^{-1} by adjusting the nitrate recycle rate q_{ir}. The controller receives a NO_3^--N concentration signal from the nitrate probe located in the second anoxic tank and has a proportional gain $K_p = 15,000$ m^3 d^{-1} per $mgNO_3^-$ L^{-1} and integral time $t_I = 0.05$ d. q_{ir} is capped at $92,230$ m^3 d^{-1}, i.e. 5×DWF.

In the closed-loop simulation scenario with DO, nitrate, and SAD_m control, coarse-bubble aeration in the membrane tank is additionally adjusted in proportion to the permeate flux rate J, as described in Maere et al. (2011). The P controller receives the permeate flow rate signal from the flow transmitter positioned on the discharge side of the permeate suction pump, calculates the value of the permeate flux and adjusts the $\mathrm{SAD_m}$ rate in proportion to J. The controller's proportional gain K_p is equal 0.015 $\mathrm{Nm^3\ h^{-1}\ m^{-2}}$ per Lmh. $\mathrm{SAD_m}$ is capped from the top and the bottom at $\mathrm{SAD_m^{min}} = 0.15\ \mathrm{Nm^3\ h^{-1}\ m^{-2}}$ and $\mathrm{SAD_m^{max}} = 0.30\ \mathrm{Nm^3\ h^{-1}\ m^{-2}}$ which correspond to permeate fluxes of 10 Lmh and 20 Lmh, respectively.

3.3. Pumping and aeration

The aeration model implemented in IBMF-MBR and its parameters are identical to the aeration model of Maere et al. (2011) implemented in BSM-MBR, however the energy consumption for pumping is calculated differently to both BSM-MBR and the COST/IWA benchmark simulation model No.1 (BSM1). Instead of using pumping energy factors representing energy consumption per $\mathrm{m^3}$ of pumped liquid, as used in the earlier benchmarks, pumping energy is calculated with Equation 1 describing the amount of work required to raise a given volume of liquid to a required height.

$$PE = \frac{60\,\rho_w\,g}{1000\,t_{simu}} \sum_{i=1}^{i=5} \frac{h_g^i + h_l^i}{\eta_i} \int_{t_0}^{t_0+t_{simu}} q_i(t)\,dt \qquad (1)$$

where $i = 1$ for waste activated sludge (WAS) flow, $i = 2$ for internal recycle flow, $i = 3$ for recirculated activated sludge (RAS) flow, $i = 4$ for pumped permeate flow and $i = 5$ for backflush flow. The parameters characterising each pumped stream are provided in Table 3.

Table 3: Values of the parameters used for pumping energy calculations with Equation 1 - Reprinted from Janus and Ulanicki (2014).

Parameter	Symbol	Unit	Flow				
			q_w	q_{int}	q_r	q_{eff}	q_b
Geometric height	h_g	m	7.0	0.50	0.50	calc	calc
Sum of losses	h_l	m	2.17	1.42	1.42	0.5	0.5
Efficiency	η	–	0.5	0.7	0.7	0.7	0.7

3.4. Fouling indices

In order to compare the operating strategies in our benchmark model with respect to fouling we indroduced two new measures of fouling which describe the increase of irreversible and reversible membrane resistance per net unit volume of permeate within a given time period. The irreversible fouling index FI_i describes the amount of irreversible resistance R_i accumulated in the last 7 days of dynamic simulation divided by the net volume of permeate discharged from the plant (see Equation 2).

$$FI_i = \frac{{R_i}^{14\text{d}} - {R_i}^{7\text{d}}}{1000 \displaystyle\int_{7\text{d}}^{14\text{d}} (q_{eff} - q_b)\, dt} = \frac{\Delta R_i}{1000\, V_{eff}^{\text{net}}} \tag{2}$$

Here, V_{eff}^{net} denotes the volume of permeate produced minus the volume of permeate used for backflushing. The reversible fouling index FI_r describes the average amount of reversible resistance R_r accumulated in one filtration cycle over the last 7 days of dynamic simulation divided by V_{eff}^{net} (see Equation 3).

$$FI_r = \frac{\displaystyle\sum_{j=1}^{N} \left({R_r}^{7\text{d}+\left(t_f+t_b\right)(j-1)+t_f} - {R_r}^{7\text{d}+\left(t_f+t_b\right)(j-1)} \right)}{1000\, N \displaystyle\int_{7\text{d}}^{14\text{d}} (q_{eff} - q_b)\, dt} = \frac{\displaystyle\sum_{j=1}^{N} \Delta R_r^j}{1000\, N\, V_{eff}^{\text{net}}} \tag{3}$$

Both fouling indices can be used to calculate the fouling cost indices FCI_i and

FCI_r describing the operational expenditures associated with mitigation of, respectively, irreversible fouling (Equation 4) and reversible fouling (Equation 5).

$$FCI_i = FI_i \cdot c_i + \frac{\mathrm{PE}^{i}_{q_{eff}}\, 7\,\mathrm{d}}{V^{\mathrm{net}}_{eff}}\, p_{kWh} \tag{4}$$

$$FCI_r = \frac{\left(\mathrm{PE}^{r}_{q_{eff}} + \mathrm{PE}_{q_{back}} + \mathrm{AE}_{\mathrm{membrane}}\right)\, 7\,\mathrm{d}}{V^{\mathrm{net}}_{eff}}\, p_{kWh} \tag{5}$$

where c_i, (€ m) denotes the financial effort required to recover $1\mathrm{m}^{-1}$ of irreversible membrane resistance, $\mathrm{PE}^{i}_{q_{eff}}$ and $\mathrm{PE}^{r}_{q_{eff}}$ (kWh d^{-1}) represent daily pumping energy requirements for permeate pumping incurred due to, respectively, irreversible and reversible fouling, and p_{kWh} (€ kWh^{-1}) is the unit price of electrical energy. Since the financial costs are not compared in our benchmark model nor in BSM-MBR, FCI_i and FCI_r calculations are not included in this paper, however the equations are still provided for further reference and for future applications of the IBMF-MBR benchmark model.

3.5. Kinetic parameters

The kinetic and stoichiometric parameters of the biological model are assigned the default values provided in Janus and Ulanicki (2015a) except 3 biopolymer kinetic and stoichiometric parameters: $f_{EPS,h}$, $f_{EPS,dh}$, and μ_{BAP}. $f_{EPS,h}$ and $f_{EPS,dh}$ were decreased, respectively from 0.18 to 0.10 gX_{EPS} g^{-1} X_H and from 0.045 to 0.025 gX_{EPS} g^{-1} X_H to reduce the production of EPS and bring the bulk liquid EPS concentrations closer to the values reported by Ahmed et al. (2007). μ_{BAP} was increased from 0.05 d^{-1} to 0.15 d^{-1} in order to lessen the dominance of biomass associated products (BAP) production over utilisation associated products (UAP) production. Simulations were performed at the same temperatures as used in BSM-MBR, i.e.

wastewater temperature T of 15°C and air temperature T_{air} of 20°C.

3.6. Membrane filtration

The membrane module is modelled with a hollow fibre module geometry of Busch et al. (2007) and with geometric dimensions provided in Janus and Ulanicki (2015c). The module is assumed to cover 100% of the tank's floor plan area. The resulting membrane packing density is equal to 49.4 m^2 m^{-3} which is slightly higher from the packing density of 46.2 m^2 m^{-3} featured in Maere et al. (2011).

The membrane is operating with 10-minute filtration periods followed by a 1-minute backflush. The module is aerated during filtration, however the aeration is switched off during backflush periods. Other membrane and fouling-specific parameters of the membrane filtration model used in the simulations are listed in Table 4.

Table 4: Parameters of the membrane filtration and fouling model applied in IBMF-MBR.

Symbol	Value	Unit	Description
R_m	3.0×10^{12}	m^{-1}	Clean membrane resistance
ΔP_{crit}	30	kPa	Threshold pressure below which no cake compression occurs
n_α	0.25	–	Dimensionless cake compressibility factor
b	6.8×10^{-2}	–	Dimensionless proportionality coefficient
k_i	1.0×10^{11}	m kg^{-1}	Irreversible fouling strength factor
γ_m	1500	d^{-1} Pa^{-1}	Proportionality constant
λ_m	2.0×10^{-6}	–	Static friction coefficient

4. Model inputs

Input files from BSM1 and BSM-MBR simulation benchmarks have been modified to take into account three new state variables, i.e. X_{EPS}, S_{UAP}, and S_{BAP} featured in IBMF-MBR. It is assumed that the influent wastewater does not contain any UAP, hence $S_{UAP} = 0$, whilst S_{BAP} makes up 70% of the influent soluble inert substrates, S_I, in BSM1 and BSM-MBR benchmarks. Influent X_{EPS} is assumed to constitute

5% of influent biomass, i.e. the sum of X_H and X_A, in BSM1 and BSM-MBR. It is also assumed that EPS and BAP contain 6% of nitrogen (N) whilst UAP are just composed of organic carbon (C). Since IBMF-MBR is based on CES-ASM1 and BSM1 and BSM-MBR are based on ASM1, composition of the influent files for IBMF-MBR has been recalculated from the former benchmark models to take into account three new biopolymer state variables and readjust some of the original state variables so that all benchmarks receive the same influent C and N loads. Values of the new influent state variables have been obtained with the following set of linear equations

$$\mathbf{x}_{inf}^{CES-ASM1} = \mathbf{A}_{inf}\,\mathbf{x}_{inf}^{ASM1} \tag{6}$$

where $\mathbf{x}_{inf}^{CES-ASM1} = (S_{BAP}, S_I, S_{ND}, X_{EPS}, X_H, X_A, X_{ND})^T$ is the vector of the influent biopolymer state variables and the recalculated influent ASM1 state variables, and $\mathbf{x}_{inf}^{ASM1} = (S_I, S_{ND}, X_H, X_A, X_{ND})^T$ is the vector of the selected influent ASM1 state variables.

The conversion matrix A_{inf} is provided below.

$$A_{inf} = \begin{pmatrix} f_{SMP}^{inf} & & & & \\ 1 - f_{SMP}^{inf} & & & & \\ -i_{XBAP}^{inf}\, f_{SMP}^{inf} & 1 & & & \\ & & f_{EPS}^{inf} & f_{EPS}^{inf} & \\ & & 1 - f_{EPS}^{inf} & & \\ & & & 1 - f_{EPS}^{inf} & \\ & & f_{EPS}^{inf}\left(i_{XB}^{inf} + i_{XEPS}^{inf}\right) & f_{EPS}^{inf}\left(i_{XB}^{inf} + i_{XEPS}^{inf}\right) & 1 \end{pmatrix} \tag{7}$$

where $f_{EPS}^{inf} = 0.05$, $f_{SMP}^{inf} = 0.7$, $i_{XB}^{inf} = 0.086$, $i_{XEPS}^{inf} = 0.06$, $i_{XBAP}^{inf} = 0.06$.

The flow-proportionally averaged influent concentrations for the IBMF-MBR

Table 5: Flow proportionally averaged influent composition for the IBMF-MBR simulation model.

Compound	Unit	Dry weather	Rain weather	Storm weather
S_I	gO_2 m^{-3}	9.00	7.78	8.41
S_S	gO_2 m^{-3}	69.50	60.13	64.93
X_I	gO_2 m^{-3}	51.20	44.30	51.92
X_S	gO_2 m^{-3}	202.32	175.05	193.32
X_H	gO_2 m^{-3}	26.76	23.15	25.89
X_A	gO_2 m^{-3}	0.00	0.00	0.00
X_{EPS}	gO_2 m^{-3}	1.41	1.22	1.36
S_{UAP}	gO_2 m^{-3}	0.00	0.00	0.00
S_{BAP}	gO_2 m^{-3}	21.00	18.17	19.62
X_P	gO_2 m^{-3}	0.00	0.00	0.00
S_O	gO_2 m^{-3}	0.00	0.00	0.00
S_{NO}	gN m^{-3}	0.00	0.00	0.00
S_{NH}	gN m^{-3}	31.56	27.30	29.48
S_{ND}	gN m^{-3}	6.95	6.01	6.49
X_{ND}	gN m^{-3}	9.37	8.10	9.10
S_{ALK}	molHCO_3^- m^{-3}	7.00	7.00	7.00
q_{ave}	m^3 d^{-1}	18446.33	21319.75	19744.72
q_{min}	m^3 d^{-1}	10000.00	10000.00	10000.00
q_{max}	m^3 d^{-1}	32180.00	52126.00	60000.00

model for all three weather scenarios are presented in Table 5. These concentrations along with the average flows were used as inputs to the benchmark model to obtain a steady-state condition and produce steady-state outputs presented in Section 5.1. In reality, all three weather scenarios exhibit a diurnal flow and load pattern as a result of changes in human activity over the course of the day. Additionally, rain and storm events include, respectively, diluting effects of rain water on wastewater constituents and increase of particulate wastewater constituents during the first storm event as a results of sediment washout from the sewer. Extensive description of these time-series data can be found in Copp (2002). These time-series data, originally used for the ASM1 model have been converted to suit the CES-ASM1 model using Equation 6.

5. Simulation results

5.1. Steady-state results

Table 6: Steady state concentrations in all reactor zones, membrane permeate and retentate stream from dry-weather open-loop simulations.

	Inf	R.1	R.2	R.3	R.4	R.5	Perm	Ret
S_I	9.00	9.00	9.00	9.00	9.00	9.00	9.00	9.00
S_S	69.50	4.53	4.24	2.91	2.51	1.90	1.90	1.90
X_I	51.20	3342.24	3342.24	4439.27	4439.27	5901.99	0.00	5901.99
X_S	202.32	64.46	60.04	34.81	27.33	24.32	0.00	24.32
X_H	26.76	1298.25	1292.43	1716.50	1716.94	2277.89	0.00	2277.89
X_A	0.00	119.73	119.29	159.87	160.18	212.86	0.00	212.86
X_{EPS}	1.41	550.59	550.32	732.31	732.56	974.03	0.00	974.03
S_{UAP}	0.00	10.31	11.10	11.65	11.59	11.97	5.99	11.97
S_{BAP}	21.00	25.81	26.54	27.64	27.29	29.92	14.96	29.92
X_P	0.00	2161.24	2162.84	2878.66	2879.53	3831.03	0.00	3831.03
S_O	0.00	0.01	0.00	1.34	1.81	7.08	7.08	7.08
S_{NO}	0.00	3.44	0.60	8.37	10.487	12.43	12.43	12.43
S_{NH}	31.56	9.50	10.23	3.18	1.248	0.23	0.23	0.23
S_{ND}	6.95	1.15	0.77	0.98	0.990	0.88	0.88	0.88
X_{ND}	9.37	4.04	4.13	2.63	2.157	2.05	0.00	2.05
S_{ALK}	7.00	5.18	5.43	4.38	4.086	3.87	3.87	3.87
X_{TSS}	211.27	5652.38	5645.37	7471.06	7466.85	9916.58	0.000	9916.58
Q	18446.33	73784.33	73784.33	129122.33	129122.33	129122.33	18286.33	55498.00

Steady-state simulation results from IBMF-MBR model in open-loop configuration and closed-loop configuration with DO, NO_3^--N and SAD_m control are listed in Tables 6 and 7, where Inf denotes the influent stream, R.1, R.2, R.3, R.4, and R.5 denote the individual bioreactors, Perm denotes the permeate stream and Ret is the retentate stream. The effluent quality in open-loop and closed-loop simulations is similar but, as shall be shown later, the treatment costs are different. SMP concentration in the membrane tank is found to be around 42 mgO_2 L^{-1} while the EPS/MLSS ratio is equal to $\sim$ 98.2 mgO_2 g^{-1} TSS. The plant produces a relatively low steady state nitrate concentration S_{NO} of about 12 mgN L^{-1} and a very low

Table 7: Steady state concentrations in all reactor zones, membrane permeate and retentate stream from dry-weather closed-loop simulations with DO, SAD_m and NO_3^--N control.

	Inf	R.1	R.2	R.3	R.4	R.5	Perm	Ret
S_I	9.00	9.00	9.00	9.00	9.00	9.00	9.00	9.00
S_S	69.50	4.35	3.34	2.90	2.55	1.94	1.94	1.9
X_I	51.20	3466.97	3466.97	4439.76	4439.76	5902.64	0.00	5902.64
X_S	202.32	61.27	58.01	35.09	28.01	24.78	0.00	24.78
X_{BH}	26.76	1329.57	1324.45	1696.30	1696.77	2251.41	0.00	2251.41
X_{BA}	0.00	122.84	122.44	158.02	158.30	210.37	0.00	210.37
X_{EPS}	1.41	565.27	565.04	724.74	724.98	963.97	0.00	963.97
S_{UAP}	0.00	10.22	10.71	11.35	11.35	11.83	5.91	11.83
S_{BAP}	21.00	25.61	26.08	27.11	26.82	29.46	14.73	29.46
X_P	0.00	2248.04	2249.49	2885.59	2886.39	3840.12	0.000	3840.12
S_O	0.00	0.01	0.00	1.69	1.50	4.49	4.49	4.49
S_{NO}	0.00	3.661	1.000	7.900	9.77	11.670	11.670	11.67
S_{NH}	31.56	8.616	9.258	3.018	1.29	0.240	0.240	0.24
S_{ND}	6.95	1.129	0.762	0.985	1.00	0.889	0.889	0.89
X_{ND}	9.37	3.886	4.008	2.648	2.20	2.081	0.000	2.08
S_{ALK}	7.00	5.100	5.336	4.397	4.14	3.930	3.930	3.93
X_{TSS}	211.27	5845.47	5839.80	7454.62	7450.66	9894.97	0.00	9894.97
Q	18446.33	83217.50	83217.50	138555.50	138555.50	129122.33	18286.33	55498.00

ammoniacal N concentration of ~ 0.25 mgN L^{-1}. The biomass is not uniformly distributed in the bioreactor but instead exhibits an upward gradient with lower MLSS concentrations of around 6 kgSS m^{-3} in the anoxic tanks and higher MLSS concentrations in the aerobic tanks and the membrane tank of, respectively ~ 7.5 kgSS m^{-3} and ~ 10 kgSS m^{-3}. What this MLSS concentration gradient along the bioreactor implies is that despite allowing a large volumetric anoxic fraction $V_{ax}/V_{tot} = 0.50$ the anoxic mass fraction in our plant is in fact very low and equals $M_{ax}/M_{tot} = 0.124$. Hence, it seems, that although membrane technology allows us to reduce aerobic volume, the benefits with regards to N and, similarly, biological phosphorus (P) removal are less obvious, at least in pre-denitrification systems with such configuration of tanks and recirculation streams as used in our benchmark model.

Effluent soluble concentrations produced from IBMF-MBR and BSM-MBR are

Table 8: Comparison of steady-state effluent soluble concentrations between IBMF-MBR and BSM-MBR.

Output	Unit	BSM-MBR		IBMF-MBR	
		Open-loop	Closed-loop*)	Open-loop	Closed-loop*)
S_I	$gO_2\ m^{-3}$	30.00	30.00	9.00	9.00
S_S	$gO_2\ m^{-3}$	0.68	0.69	1.90	1.94
S_{UAP}	$gO_2\ m^{-3}$	–	–	5.99	5.91
S_{BAP}	$gO_2\ m^{-3}$	–	–	14.96	14.73
S_O	$gO_2\ m^{-3}$	7.69	5.19	7.08	4.49
S_{NO}	$gN\ m^{-3}$	12.03	11.71	12.43	11.67
S_{NH}	$gN\ m^{-3}$	0.076	0.080	0.23	0.24
S_{ND}	$gN\ m^{-3}$	0.59	0.59	0.88	0.89
S_{ALK}	$molHCO_3^-\ m^{-3}$	3.89	3.92	3.87	3.93

*) DO, NO_3^--N, and SAD_m control

compared in Table 8. The results show that the outputs of both models are very similar with minor differences in S_S, S_{NO} and S_{NH}. Particulate components are omitted in the table as they all have zero concentrations.

5.2. Dynamic results

Dynamic simulations were performed with BSM-MBR and IBMF-MBR models in dry-, rain- and storm-weather under four levels of process control: (a) open-loop, (b) closed-loop with DO control, (c) closed-loop with DO and NO_3^--N control and (d) closed-loop with DO, NO_3^--N and SAD_m control. Alike in BSM1 and BSM-MBR benchmarks the results constitute the last 7 days of outputs.

The flow-proportionally averaged effluent concentrations from open-loop and closed loop simulations under all three weather scenarios are listed, respectively in Tables 9 and 10. Alike in steady-state simulations, closed loop dynamic simulation refers to the simulation scenario with DO, SAD_m and NO_3^--N control. The results show that IBMF-MBR predicts, on average, ~ 1 mgN L^{-1} higher effluent total nitrogen (TN) than the ASM1-based BSM-MBR due to slightly higher produced effluent NO_3^--N and ammoniacal nitrogen (NH_4^+-N) concentrations. Effluent total Kjeldahl nitrogen (TKN) produced by IBMF-MBR is again about 1.5 mgN L^{-1} higher than those in the BSM-MBR benchmark model as a result of higher NH_4^+-N and soluble organic N concentrations. The rest of the effluent state and composite variables in both models have similar values except soluble inert organics (S_I) which are lower in IBMF-MBR due to lower influent S_I concentrations which had been reduced in order to accommodate three new biopolymer state variables in the influent (input) files.

The selected effluent concentrations from the last 7 days of dynamic simulation under different weather conditions and process control variants are presented in Figures 3-6. Figure 3 indicates that, in response to the changes in the influent flow rate, MLSS concentrations in the individual reactors fluctuate significantly as the biomass is shifted downstream under high flows and then returned upstream with RAS flow after the influent flow rate has subsided. This behaviour is observed during the periods when the flow of wastewater is large enough for the flux of suspended solids along the bioreactor to exceed the sludge return rate. As a result, during these periods, the sludge is shifted downstream to the membrane tank. Unfortunately, these increased sludge loading events in the membrane tank usually coincide with high permeate fluxes, ultimately leading to a simultaneous increase in the rates of reversible fouling and irreversible fouling, the latter, as shown in Janus and Ulanicki (2015b), increasing exponentially with the permeate flux.

Figure 4 indicates that DO concentration in both aerobic tanks fluctuates significantly in an open-loop process control scenario. Once automatic DO control is switched on, DO concentration in the second aerobic tank is kept at an almost steady level of 1.5 mgO_2 L^{-1} whilst S_O in the first aerobic tank varies between 1.4 mgO_2 L^{-1}

Table 9: Flow proportionally averaged effluent concentrations from dynamic open-loop simulations with BSM-MBR and IBMF-MBR in dry-, rain- and storm-weather.

Variable	Unit	BSM-MBR			IBMF-MBR		
		Dry	Rain	Storm	Dry	Rain	Storm
Effluent state variables							
S_I	$gO_2\ m^{-3}$	30.00	22.86	26.30	9.00	6.86	7.89
S_S	$gO_2\ m^{-3}$	0.73	0.75	0.76	1.96	1.97	2.02
X_I	$gO_2\ m^{-3}$	0.00	0.00	0.00	0.00	0.00	0.00
X_S	$gO_2\ m^{-3}$	0.00	0.00	0.00	0.00	0.00	0.00
X_H	$gO_2\ m^{-3}$	0.00	0.00	0.00	0.00	0.00	0.00
X_A	$gO_2\ m^{-3}$	0.00	0.00	0.00	0.00	0.00	0.00
X_{EPS}	$gO_2\ m^{-3}$	–	–	–	0.00	0.00	0.00
S_{UAP}	$gO_2\ m^{-3}$	–	–	–	6.20	6.05	6.30
S_{BAP}	$gO_2\ m^{-3}$	–	–	–	15.26	13.68	14.63
X_P	$gO_2\ m^{-3}$	0.00	0.00	0.00	0.00	0.00	0.00
S_O	$gO_2\ m^{-3}$	6.97	6.32	6.27	5.96	5.35	5.23
S_{NO}	$gN\ m^{-3}$	12.21	10.76	11.26	12.74	11.14	11.63
S_{NH}	$gN\ m^{-3}$	0.15	0.15	0.17	0.45	0.44	0.54
S_{ND}	$gN\ m^{-3}$	0.61	0.62	0.64	0.89	0.89	0.90
X_{ND}	$gN\ m^{-3}$	0.00	0.00	0.00	0.00	0.00	0.00
S_{ALK}	$molHCO_3^-\ m^{-3}$	3.88	4.52	4.23	3.87	4.52	4.23
Effluent composite variables							
TSS	$g\ m^{-3}$	0.00	0.00	0.00	0.00	0.00	0.00
TKN	$gN\ m^{-3}$	0.76	0.78	0.81	2.25	2.15	2.31
TN	$gN\ m^{-3}$	12.98	11.54	12.07	14.99	13.29	13.94
COD	$gO_2\ m^{-3}$	30.73	23.61	27.06	32.43	28.55	30.84
BOD_5	$gO_2\ m^{-3}$	0.18	0.19	0.19	0.49	0.49	0.50

and 2.1 $mgO_2\ L^{-1}$. Introduction of an automatic DO control scheme prevents over-aeration of the bulk liquid in low organic and N loading periods, decreases the effluent NH_4^+-N concentration, albeit at already very low level, but also leads to an increase in effluent TN concentrations, as can be seen when we cross examine Table 11 and Table 12. This behaviour can be explained as follows. The system has a high aerobic sludge retention time (SRT), hence nitrification rates are ultimately high whilst nitrogen removal is limited by denitrification. Under open-loop operation, fluctuation of DO concentration in both aerobic tanks leads to a temporary cyclic development

Table 10: Flow proportionally averaged effluent concentrations from dynamic closed-loop simulations (DO, NO_3^--N and SAD_m control) with BSM-MBR and IBMF-MBR in dry-, rain- and storm-weather.

Variable	Unit	BSM-MBR			IBMF-MBR		
		Dry	Rain	Storm	Dry	Rain	Storm
Effluent state variables							
S_I	$gO_2\ m^{-3}$	30.00	22.86	26.30	9.00	6.86	7.89
S_S	$gO_2\ m^{-3}$	0.70	0.72	0.73	2.01	2.03	2.07
X_I	$gO_2\ m^{-3}$	0.00	0.00	0.00	0.00	0.00	0.00
X_S	$gO_2\ m^{-3}$	0.00	0.00	0.00	0.00	0.00	0.00
X_H	$gO_2\ m^{-3}$	0.00	0.00	0.00	0.00	0.00	0.00
X_A	$gO_2\ m^{-3}$	0.00	0.00	0.00	0.00	0.00	0.00
X_{EPS}	$gO_2\ m^{-3}$	–	–	–	0.00	0.00	0.00
S_{UAP}	$gO_2\ m^{-3}$	–	–	–	6.07	5.95	6.09
S_{BAP}	$gO_2\ m^{-3}$	–	–	–	14.93	13.48	14.14
X_P	$gO_2\ m^{-3}$	0.00	0.00	0.00	0.0	0.00	0.00
S_O	$gO_2\ m^{-3}$	5.33	5.65	5.20	3.90	4.29	3.75
S_{NO}	$gN\ m^{-3}$	12.19	10.35	11.15	11.89	10.27	10.86
S_{NH}	$gN\ m^{-3}$	0.10	0.10	0.10	0.39	0.37	0.40
S_{ND}	$gN\ m^{-3}$	0.60	0.61	0.62	0.91	0.91	0.92
X_{ND}	$gN\ m^{-3}$	0.00	0.00	0.00	0.00	0.00	0.00
S_{ALK}	$molHCO_3^-\ m^{-3}$	3.88	4.24	4.23	3.93	4.58	4.28
Effluent composite variables							
TSS	$g\ m^{-3}$	0.00	0.00	0.00	0.00	0.00	0.00
TKN	$gN\ m^{-3}$	0.70	0.71	0.72	2.19	2.09	2.17
TN	$gN\ m^{-3}$	12.89	11.06	11.87	14.08	12.36	13.03
COD	$gO_2\ m^{-3}$	30.70	23.58	27.03	32.00	28.32	30.20
BOD_5	$gO_2\ m^{-3}$	0.18	0.18	0.18	0.50	0.51	0.52

of anoxic conditions inside both aerobic tanks thus increasing denitrification capacity in the system. Once DO control is switched on, both aerobic tanks become fully aerobic at all times reducing the overall anoxic mass fraction in the system and hence its denitrification potential. The simulations thus show that although DO control offers benefits, usually in the form of energy savings, it may cause some detrimental effects in the plant such as unwanted reduction of denitrification potential, as in case of our system.

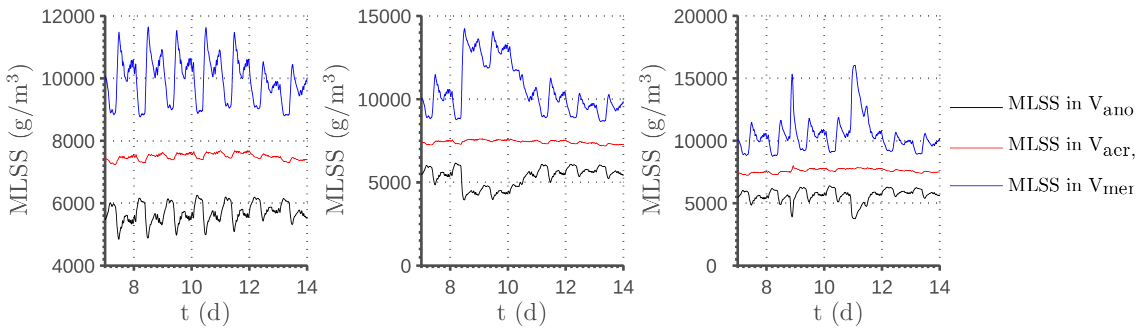

Figure 3: MLSS concentrations in open-loop simulation during (from left to right) dry-, rain- and storm-weather conditions.

DO concentration in the membrane tank fluctuates significantly between nearly 0 mgO_2 L^{-1} to almost its saturation concentration of $\sim$ 9 mgO_2 L^{-1}. At such high oxygen concentrations, significant amounts of oxygen are being carried over into the anoxic zones with RAS stream, what in turn impairs denitrification. Once SAD_m control is switched on DO concentration in the membrane tank is reduced, what in turn decreases the ingress of the mass of oxygen into anoxic tanks, ultimately leading to reduction in effluent TN concentrations and the amount of time at violation for TN. The level of improvement in TN removal with introduction of SAD_m control can be judged from Table 13. Impact of SAD_m control on N removal is one of the examples how operation of the membrane might have an impact on the performance of an entire plant.

As already mentioned, effluent NH_4^+-N concentration is very low at all times during all weather conditions and under all operating scenarios due to high nitrification capacity of the system. As can be seen in Figure 5 at no point in time effluent NH_4^+-N exceeds the effluent NH_4^+-N constraint $S_{NH,max}$ = 4 mgN L^{-1} whilst S_{NH} is below 1 mgN L^{-1} at around $\sim$ 90% of the time.

On the other hand, effluent total nitrogen (TN) concentration exceeds the effluent

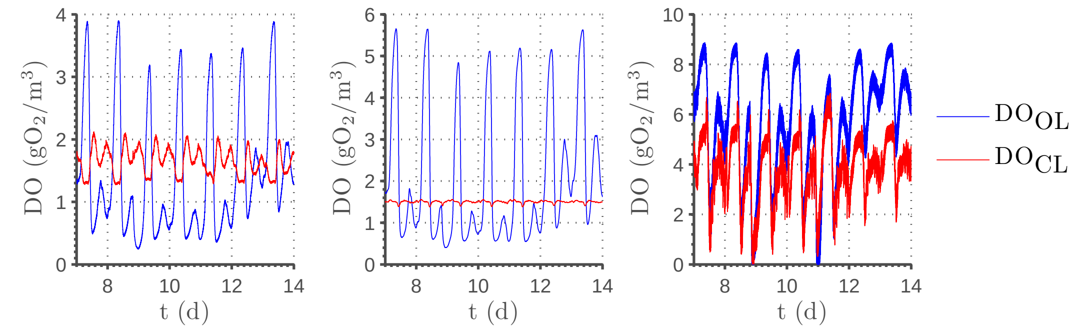

Figure 4: DO concentrations during in the (from left to righ) first aerobic tank, second aerobic tank, and membrane tank in dry-weather conditions.

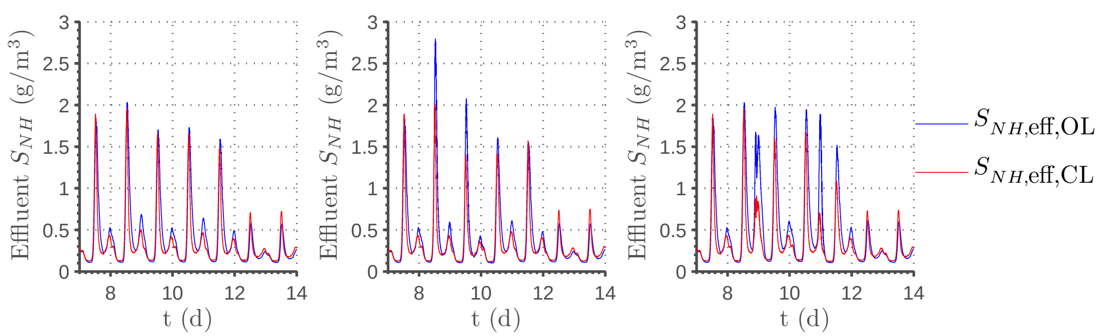

Figure 5: Effluent NH_4^+-N concentrations during (from left to right) dry-, rain- and storm-weather conditions.

TN constraint of 18 mgN L^{-1} at some point of time in each weather scenario and under each process control variant, as demonstrated in Figure 6. It is clear that although the plant achieves a complete and stable nitrification, N removal efficiency is rather low in comparison to nitrification due to slow denitrification rates as a result of high SRT and ingress of DO mass from the membrane tank to the first anoxic tank.

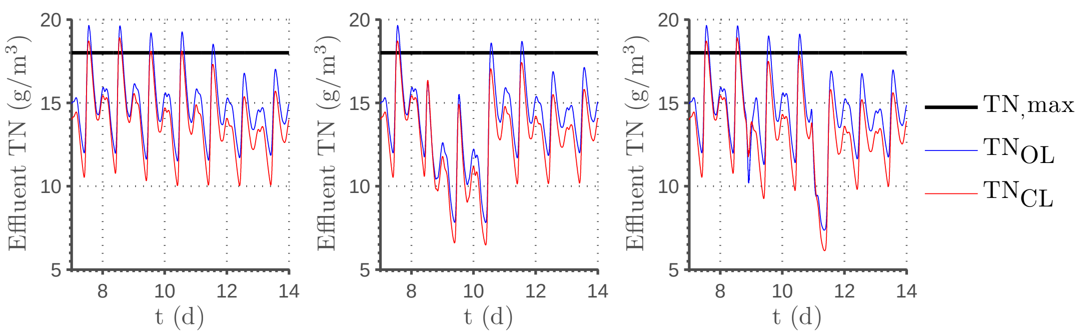

Figure 6: Effluent TN concentrations during (from left to right) dry-, rain- and storm-weather conditions - Reprinted from Janus and Ulanicki (2014).

5.3. Effluent quality measures and cost performance

Performance of the BSM-MBR benchmark simulation model and IBMF-MBR in each weather scenario and under each level of process control is summarised in Tables 11, 12, 13 and 14 which correspond, as mentioned earlier on, to the following process control scenarios: open-loop, closed-loop with DO control, closed-loop with DO and SAD_m control, and closed-loop with DO, SAD_m and NO_3^--N control.

IBMF-MBR produces higher effluent TN concentrations than BSM-MBR, as indicated by the 95-th percentile of the total nitrogen concentration (TN_{95}), number of TN consent limit violations, and % of time under violation. While BSM-MBR produces no TN violations under the open-loop scenario and under the closed-loop scenario with DO, SAD_m and NO_3^--N control, IBMF-MBR exceeds the TN constraint under all weather conditions and under all levels of process control despite having a higher anoxic volume fraction. Effluent TN_{95} concentration produced by BSM-MBR is on average about 2 mgN L^{-1} lower than in IBMF-MBR. As already mentioned in Section 2, higher effluent TN concentrations in IBMF-MBR are a direct result of lower denitrification rates in the CES-ASM1 biological model compared to ASM1. In turn, lower denitrification rates are a consequence of an addition of biopolymer kinetics into the biological model which alter the death-regeneration loop in ASM1 causing less of readily biodegradable substrates to be produced during bacterial lysis. Although not validated numerically, lower denitrification rates in CES-ASM1 are theoretically and practically justified as ASM1 was found to overestimate denitrification rates in high SRT systems where the death-regeneration model perpetually produces readily biodegradable organic substrates in the bioreactor.

IBMF-MBR also generates less waste activated sludge (WAS) leading to $\sim 20\%$ lower observed sludge yield (Y_{obs}) and therefore, higher aerobic and total SRT. Whilst energy demand for fine bubble aeration is slightly higher in IBMF-MBR, energy demand for air scouring is less due to lower installed membrane area. In consequence, similar overall energy requirements for aeration are predicted in both models. Mixing energy requirement is $\sim 24\%$ higher in IBMF-MBR due to larger total anoxic tank volume, whilst energy consumption for pumping is significantly lower due to lower energy requirements for permeate pumping, which were found to be grossly overestimated in BSM-MBR. The calculated transmembrane pressures (TMPs) in IBMF-MBR are ~ 8 times lower from the values predicted in the BSM-MBR model despite rather average, for ultrafiltration (UF) modules, permeabilities of 80–100 Lmh bar^{-1}, due to very conservative permeate fluxes of 8–20 Lmh in dry-weather and up to 32 Lmh and 38 Lmh in rain and storm weather, respectively.

5.4. Biopolymer production and membrane fouling

Bulk liquid SMP concentrations in the membrane tank under all three weather scenarios are plotted in Figure 7 which indicates that S_{UAP} and S_{BAP} vary rather moderately in time in response to diurnal changes in influent load during dry weather and as a result of dilution effects during rain and storm weather. Since CES-ASM1, similarly to other published biopolymer ASM models, does not describe the mechanisms of biopolymer production in response to stress conditions such as extreme DO concentrations, salinity, pH, changes in the type of organic substrates, toxic effects, shear stress, etc. these system dynamics have not been captured in IBMF-MBR. Hence, the simulations only show how dynamic changes in influent flow and composition alter normal Monod-based substrate limiting SMP dynamics and these effects seem to be rather insignificant to have an observable effect on membrane fouling. It is likely that a full-scale WWTP might experience additional SMP dynamics under time varying conditions in response to environmental stress and thus, variations in bulk liquid SMP concentrations might actually be larger, but this is the topic for further research.

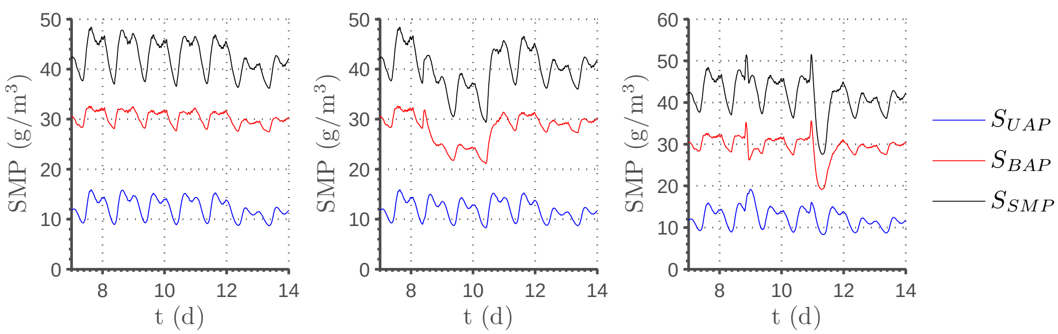

Figure 7: SMP concentrations in the membrane bioreactor during (from left to right) dry-, rain- and storm-weather conditions.

Figure 8 shows how irreversible fouling resistance (R_i) and SMP/MLSS ratio in the membrane tank change in time in all three weather scenarios. If we look at sub-figure (a) we can see that whilst under dry-weather conditions R_i increases slowly and steadily at the rate of about 1.10×10^{-2} m kg^{-1} h^{-1}, under elevated flow conditions in wet periods the rate of R_i increase is up to four times larger and around 4.58×10^{-2} m kg^{-1} h^{-1} in rain weather, and up to ~ 0.21 m kg^{-1} h^{-1} in storm weather. If we then look at sub-figure (b) presenting the SMP/MLSS ratio in the membrane tank, we can see that the rate of irreversible fouling coincides with a decrease in the SMP/MLSS ratio. The results thus indicate that the rate of irreversible fouling depends much more on flux than on SMP concentrations which, in our case, decrease in wet-periods due to dilution with rain and storm water.

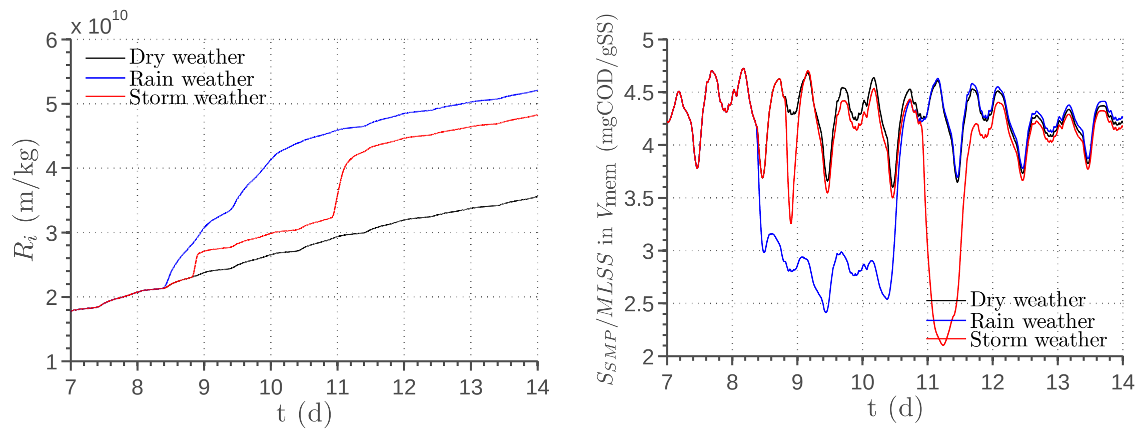

Figure 8: (a) Resistance due to irreversible fouling R_i and (b) SMP fraction in MLSS vs. time during open-loop simulation in dry-, wet-, and storm-weather conditions - Reprinted from Janus and Ulanicki (2014).

As explained in Janus and Ulanicki (2015b), specific cake resistance (α_c) is calculated with the equation of Ahmed et al. (2007) which has been additionally modified to include a proportionality coefficient m that has been assigned an arbitrary value of 10 in order to raise the calculated α_c values to a level leading to sufficiently high 'observable' fouling levels in the simulation model. As shown in Figure 9, the changes in

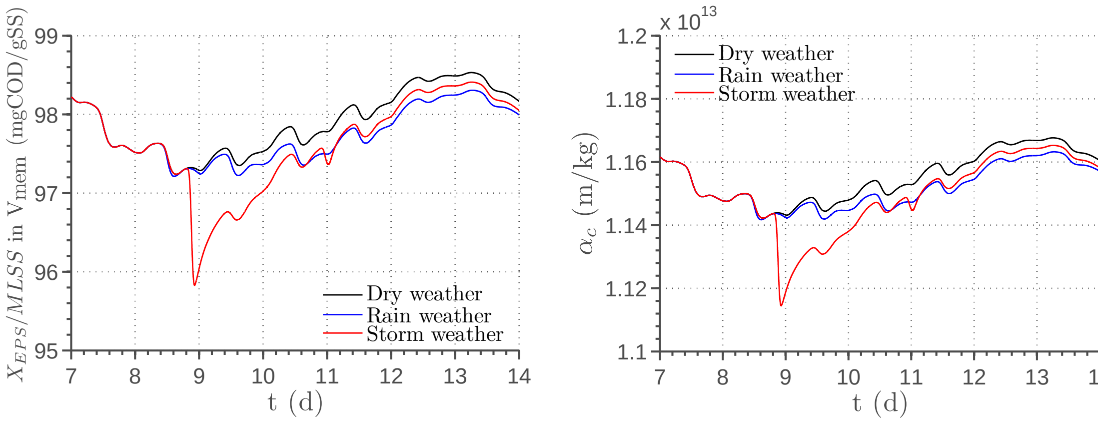

Figure 9: (a) EPS fraction in MLSS and (b) specific cake resistance α_c vs. time during the open-loop simulation in dry-, wet-, and storm-weather conditions - Reprinted from Janus and Ulanicki (2014).

α_c are proportional to the EPS content in the activated sludge due to a linear nature of Ahmed et al.'s equation. However, as X_{EPS} does not change much over the course of the simulations, α_c remains at a relatively constant value of $\sim 1.12 - 1.16$ m kg^{-1}. Although, as shown in Janus and Ulanicki (2015a), under steady state conditions the operating parameters such as DO or SRT have a noticeable effect on the EPS content in activated sludge and hence α_c, the EPS dynamics with respect to DO and temperature are slow. Hence, as pointed out above, the temporal variability of EPS content in the activated sludge is therefore small. Since the EPS production kinetics in our model are based on the standard Monod equation, similarly to SMP kinetics, the model excludes the effects of possible additional dynamics such as release of EPS in response to shock loading, toxicity, salinity etc. which might additionally affect the bulk liquid EPS concentrations and thus, α_c. Nevertheless, production of biopolymers under highly dynamic conditions is a topic for further research and therefore shall not be considered in this publication.

Figure 10 shows the calculated TMPs for a selected simulation time period under two control scenarios: (a) open-loop and (b) closed-loop with the SAD_m controller adjusting the amount of airflow in proportion to the permeate flux (Maere et al., 2011). Coarse bubble aeration reduces trans-membrane pressure (TMP) by creating shear on the cake surface which leads to cake detachment. As the rate of cake detachment is also proportional to cake thickness, a steady-state cake thickness ultimately develops for a given flux and air scouring rate. Upon reaching that thickness TMP will reach a plateau resulting in concave down pressure gradients, as shown in Figure 10. The figure demonstrates how air scouring affects TMP in the model. In our case the amount of air scouring in the open-loop scenario is excessive and thus energy is wasted on aeration without leading to further reduction in TMP. Once SAD_m control is applied, energy demand for coarse bubble aeration reduces by about a third whilst reversible fouling under low flux rates increases only slightly but is still insignificantly small compared to the overall membrane resistance, hence indicating a signiticant potential for energy savings. The above case study shows how the simulation model can be used for energy optimisation in MBR plants by testing different control scenarios, such as this simple feedback air scouring control, and demonstrates how addition of membrane fouling into BSM-MBR benchmark model, on top of biopolymer kinetics, expands its capabilities.

5.5. Energy consumption

Unit energy consumption values per m^3 of treated wastewater calculated from IBMF-MBR and BSM-MBR, and measured on three full-scale MBR plants are compared in Table 15, which extends the table originally published in Maere et al. (2011).

The energy demand predicted by IBMF-MBR in the open-loop configuration is similar to the energy consumption estimated by BSM-MBR, apart from the earlier mentioned energy for permeate pumping, which is the lowest among all effluent

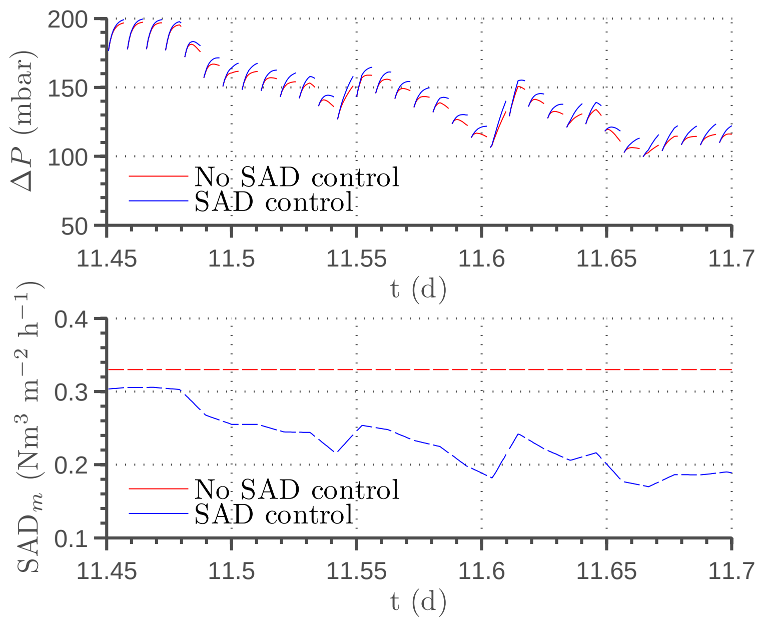

Figure 10: TMP gradients in filtration cycles for a selected time period in a simulation scenario with and without SAD_m control.

pumping energy values listed in Table 15. The reasons for this are two-fold. First, the energy costs in BSM-MBR are calculated using previously assumed unit energy consumption factors per m^3 of pumped liquid, whilst in IBMF-MBR the permeate pumping costs are directly calculated from the pumping energy equation (see Equation 1) in which the pumping head is given or, in the case of permeate pumping, calculated from the TMP values predicted by the fouling model. Since the permeate fluxes under dry-weather conditions are at the lower end of sustainable long-term fluxes used with this type of membranes, very low pressure losses across the membrane calculated by the fouling model are justifiable whilst, at the same time, the unit permeate pumping cost assumed in BSM-MBR seems to be overestimated. Second, the effects of irreversible fouling on the overall operational costs cannot be evaluated in such a short time scale as 14 days due to very slow dynamics of irreversible fouling under sustainable fluxes. The only plausible way to include the effects of irreversible fouling over a longer time period in our short-term simulation would be either to specify an initial condition for the membrane resistance which represented a typical ‘average’ membrane resistance over its entire life-span or to extrapolate the contribution of irreversible fouling into a longer period of time using the calcualated irreversible fouling rates. It is also tempting to extend the simulation horizon to a period of a few months in order to quantify the overall permeate pumping costs, but such a long-term simulation would necessitate an appropriately designed simulation scenario which would take into account the variability in the influent flow, influent load, and temperature, and which would require a careful selection of a sequence of dry- and wet-weather conditions.

Table 11: Comparison of dynamic open-loop effluent quality and operating cost performance criteria between BSM-MBR and IBMF-MBR models.

Criterion	Unit	BSM-MBR			IBMF-MBR		
		Dry	Rain	Storm	Dry	Rain	Storm
I.Q.	kgPU d^{-1}	52115.2	52115.2	54074.5	52052.1	52050.2	54029.5
E.Q.	kgPU d^{-1}	3216.9	3423.6	3423.6	4177.5	4935.9	4544.6
$S_{NH,95}$	gN m^{-3}	0.475	0.473	0.491	1.42	1.40	1.59
TN_{95}	gN m^{-3}	16.49	15.42	16.32	18.64	17.73	18.55
TSS_{95}	g m^{-3}	0	0	0	0	0	0
COD_{95}	gO_2 m^{-3}	30.90	30.80	30.86	34.78	34.31	35.16
$BOD_{5,95}$	gO_2 m^{-3}	0.225	0.232	0.237	0.605	0.610	0.638
$S_{NH,\text{violations}}$	–	0	0	0	0	0	0
(4 gN m^{-3})	% of time	0	0	0	0	0	0
$TN_{\text{violations}}$	–	0	0	0	5	3	4
(18 gN m^{-3})	% of time	0	0	0	8.16	4.31	6.87
$BOD_{5,\text{violations}}$	–	0	0	0	0	0	0
(10 gO_2 m^{-3})	% of time	0	0	0	0	0	0
$COD_{\text{violations}}$	–	0	0	0	0	0	0
(100 gO_2 m^{-3})	% of time	0	0	0	0	0	0
$TSS_{\text{violations}}$	–	0	0	0	0	0	0
(30 g m^{-3})	% of time	0	0	0	0	0	0
SP_{tot}	kgTSS d^{-1}	1971.2	1982.9	2198.5	1590.1	1587.6	1772.0
SP_{disp}	kgTSS d^{-1}	1971.2	1982.9	2198.5	1590.1	1587.6	1772.0
$AE_{\text{bioreactor}}$	kWh d^{-1}	3878.6	3878.6	3878.6	4075.6	4075.6	4075.6
AE_{membrane}	kWh d^{-1}	9680.7	9680.7	9680.7	9018.1	9018.1	9018.1
AE_{total}	kWh d^{-1}	13559.3	13559.3	13559.3	13093.7	13093.7	13093.7
PE_{total}	kWh d^{-1}	2209.2	2639.6	2403.2	1023.6	1128.3	1078.2
PE_{sludge}	kWh d^{-1}	840.1	840.1	840.1	835.2	835.2	835.2
PE_{permeate}	kWh d^{-1}	1369.2	1800.0	1563.2	188.33	293.03	243.00
PE_{q_w}	kWh d^{-1}	Not recorded	Not recorded	Not recorded	8.00	8.00	8.00
$PE_{q_{int}}$	kWh d^{-1}				413.61	413.61	413.61
PE_{q_r}	kWh d^{-1}				413.61	413.61	413.61
$PE_{q_{eff}}$	kWh d^{-1}				145.94	250.53	200.55
$PE_{q_{back}}$	kWh d^{-1}				42.39	42.50	42.25
ME	kWh d^{-1}	576	576	576	714.38	714.38	714.38
OCI	–	26200.4	26690.0	27531.2	22763.9	22856.1	23728.2
Total SRT	d	27.51	25.90	26.83	33.38	31.24	32.47
Aerobic SRT	d	18.85	18.17	18.56	20.41	19.67	20.09
Y_{obs}	–	0.700	0.743	0.732	0.565	0.603	0.591
FI_i	m^{-1} L^{-1}				4616.9	6380.8	6715.5
FI_r	m^{-1} L^{-1}				30334.2	33228.0	32855.5

Table 12: Comparison of dynamic closed-loop effluent quality and operating cost performance criteria between BSM-MBR and IBMF-MBR models with DO control.

Criterion	Unit	BSM-MBR			IBMF-MBR		
		Dry	Rain	Storm	Dry	Rain	Storm
I.Q.	kgPU d^{-1}	52115.4	52115.4	54074.5	52052.1	52050.2	54029.5
E.Q.	kgPU d^{-1}	3222.5	3714.4	3456.8	4145.9	4894.3	4504.4
$S_{NH,95}$	gN m^{-3}	0.169	0.175	0.176	0.784	0.783	0.747
TN_{95}	gN m^{-3}	17.43	16.18	17.23	19.62	18.52	19.54
TSS_{95}	g m^{-3}	0	0	0	0	0	0
COD_{95}	gO_2 m^{-3}	30.82	30.75	30.78	34.13	33.60	34.49
$BOD_{5,95}$	gO_2 m^{-3}	0.205	0.210	0.215	0.584	0.591	0.612
$S_{NH,\text{violations}}$	–	0	0	0	0	0	0
(4 gN m^{-3})	% of time	0	0	0	0	0	0
$TN_{\text{violations}}$	–	4	1	4	5	3	5
(18 gN m^{-3})	% of time	2.38	0.743	2.53	11.06	6.11	10.00
$BOD_{5,\text{violations}}$	–	0	0	0	0	0	0
(10 gO_2 m^{-3})	% of time	0	0	0	0	0	0
$COD_{\text{violations}}$	–	0	0	0	0	0	0
(100 gO_2 m^{-3})	% of time	0	0	0	0	0	0
$TSS_{\text{violations}}$	–	0	0	0	0	0	0
(30 g m^{-3})	% of time	0	0	0	0	0	0
SP_{tot}	kgTSS d^{-1}	1978.2	1990.6	2182.1	1588.4	1584.7	1764.3
SP_{disp}	kgTSS d^{-1}	1978.2	1990.6	2182.1	1588.4	1584.7	1764.3
$AE_{bioreactor}$	kWh d^{-1}	3834.3	3791.5	3945.3	4070.6	3981.4	4169.5
$AE_{membrane}$	kWh d^{-1}	9680.7	9680.7	9680.7	9018.1	9018.1	9018.1
AE_{total}	kWh d^{-1}	13515.0	13472.2	13626.0	13088.7	12999.5	13187.6
PE_{total}	kWh d^{-1}	2209.2	2639.6	2403.2	1023.5	1128.2	1078.2
PE_{sludge}	kWh d^{-1}	840.1	840.1	840.1	835.22	835.22	835.22
$PE_{permeate}$	kWh d^{-1}	1369.2	1799.5	1563.2	188.32	293.01	242.98
PE_{q_w}	kWh d^{-1}	Not recorded	Not recorded	Not recorded	8.00	8.00	8.00
$PE_{q_{int}}$	kWh d^{-1}				413.61	413.61	413.61
PE_{q_r}	kWh d^{-1}				413.61	413.61	413.61
$PE_{q_{eff}}$	kWh d^{-1}				145.93	250.52	200.54
$PE_{q_{back}}$	kWh d^{-1}				42.39	42.49	42.44
ME	kWh d^{-1}	576	576	576	714.38	714.38	714.38
OCI	–	26191.3	26640.8	27505.8	23954.9	22765.5	25123.1
Total SRT	d	27.51	25.89	26.83	33.38	31.24	32.48
Aerobic SRT	d	18.85	18.17	18.56	20.41	19.67	20.10
Y_{obs}	–	0.702	0.744	0.732	0.565	0.603	0.591
FI_i	m^{-1} L^{-1}				4532.0	6311.2	6473.7
FI_r	m^{-1} L^{-1}				30363.6	33256.0	32897.2

Table 13: Comparison of dynamic closed-loop effluent quality and operating cost performance criteria between BSM-MBR and IBMF-MBR models with DO and SAD_m control.

Criterion	Unit	BSM-MBR			IBMF-MBR		
		Dry	Rain	Storm	Dry	Rain	Storm
I.Q.	kgPU d^{-1}	52115.4	52115.4	54074.6	52052.1	52050.2	54029.5
E.Q.	kgPU d^{-1}	3197.2	3696.0	3432.0	4112.4	4871.0	4470.9
$S_{NH,95}$	gN m^{-3}	0.174	0.179	0.178	0.882	0.842	0.815
TN_{95}	gN m^{-3}	17.32	16.08	17.12	19.31	18.26	19.22
TSS_{95}	g m^{-3}	0	0	0	0	0	0
COD_{95}	gO_2 m^{-3}	30.82	30.75	30.79	34.28	33.76	34.62
$BOD_{5,95}$	gO_2 m^{-3}	0.205	0.211	0.216	0.586	0.592	0.614
$S_{NH,\text{violations}}$	–	0	0	0	0	0	0
(4 gN m^{-3})	% of time	0	0	0	0	0	0
$TN_{\text{violations}}$	–	3	1	3	5	3	5
(18 gN m^{-3})	% of time	1.63	0.594	1.63	10.16	5.56	8.81
$BOD_{5,\text{violations}}$	–	0	0	0	0	0	0
(10 gO_2 m^{-3})	% of time	0	0	0	0	0	0
$COD_{\text{violations}}$	–	0	0	0	0	0	0
(100 gO_2 m^{-3})	% of time	0	0	0	0	0	0
$TSS_{\text{violations}}$	–	0	0	0	0	0	0
(30 g m^{-3})	% of time	0	0	0	0	0	0
SP_{tot}	kgTSS d^{-1}	1977.1	1991.0	2181.2	1587.7	1584.7	1763.4
SP_{disp}	kgTSS d^{-1}	1977.1	1991.0	2181.2	1587.7	1584.7	1763.4
$AE_{\text{bioreactor}}$	kWh d^{-1}	3911.8	3848.2	4007.9	4152.4	4039.7	4246.2
AE_{membrane}	kWh d^{-1}	5597.0	6647.8	5970.9	5469.5	6409.9	5809.3
AE_{total}	kWh d^{-1}	9508.9	10486.0	9988.8	9621.9	10449.6	10055.7
PE_{total}	kWh d^{-1}	2209.2	2639.6	2403.2	1025.5	1129.7	1080.0
PE_{sludge}	kWh d^{-1}	840.07	840.07	840.07	835.22	835.22	835.22
PE_{permeate}	kWh d^{-1}	1396.2	1799.5	1563.2	190.29	294.43	244.8
PE_{q_w}	kWh d^{-1}	Not recorded	Not recorded	Not recorded	8.00	8.00	8.00
$PE_{q_{int}}$	kWh d^{-1}				413.61	413.61	413.61
PE_{q_r}	kWh d^{-1}				413.61	413.61	413.61
$PE_{q_{eff}}$	kWh d^{-1}				147.90	251.93	202.36
$PE_{q_{back}}$	kWh d^{-1}				42.39	42.49	42.44
ME	kWh d^{-1}	576	576	576	714.38	714.38	714.38
OCI	–	22179.6	23666.5	23864.1	19301.0	20217.2	20667.1
Total SRT	d	27.51	25.89	26.83	33.38	31.24	32.48
Aerobic SRT	d	18.85	18.17	18.56	20.41	19.67	20.10
Y_{obs}	–	0.701	0.744	0.732	0.565	0.603	0.591
FI_i	m^{-1} L^{-1}				4566.2	6330.0	6515.0
FI_r	m^{-1} L^{-1}				72730.4	55404.1	65751.0

Table 14: Comparison of dynamic closed-loop effluent quality and operating cost performance criteria between BSM-MBR and IBMF-MBR models with DO, SAD_m and NO_3^--N control.

Criterion	Unit	BSM-MBR			IBMF-MBR		
		Dry	Rain	Storm	Dry	Rain	Storm
I.Q.	kgPU d^{-1}	52115.4	52115.4	54074.5	52052.1	52050.2	54029.5
E.Q.	kgPU d^{-1}	3174.8	3569.5	3345.7	3980.8	4679.1	4280.6
$S_{NH,95}$	gN m^{-3}	0.191	0.207	0.201	1.16	1.07	1.05
TN_{95}	gN m^{-3}	16.72	15.22	16.48	17.82	16.64	17.45
TSS_{95}	g m^{-3}	0	0	0	0	0	0
COD_{95}	gO_2 m^{-3}	30.80	30.75	30.79	34.10	33.61	34.50
$BOD_{5,95}$	gO_2 m^{-3}	0.200	0.206	0.211	0.609	0.624	0.641
$S_{NH,\text{violations}}$	–	0	0	0	0	0	0
(4 gN m^{-3})	% of time	0	0	0	0	0	0
$TN_{\text{violations}}$	–	0	0	0	4	1	2
(18 gN m^{-3})	% of time	0	0	0	3.90	1.38	2.89
$BOD_{5,\text{violations}}$	–	0	0	0	0	0	0
(10 gO_2 m^{-3})	% of time	0	0	0	0	0	0
$COD_{\text{violations}}$	–	0	0	0	0	0	0
(100 gO_2 m^{-3})	% of time	0	0	0	0	0	0
$TSS_{\text{violations}}$	–	0	0	0	0	0	0
(30 g m^{-3})	% of time	0	0	0	0	0	0
SP_{tot}	kgTSS d^{-1}	1978.2	1992.2	2180.5	1584.5	1577.0	1757.1
SP_{disp}	kgTSS d^{-1}	1978.2	1992.2	2180.5	1584.5	1577.0	1757.1
$AE_{\text{bioreactor}}$	kWh d^{-1}	3897.8	3806.9	3974.1	4096.4	3951.3	4159.2
AE_{membrane}	kWh d^{-1}	5596.9	6647.6	5970.4	5469.4	6410.0	5809.2
AE_{total}	kWh d^{-1}	9494.7	10454.5	9944.5	9565.8	10361.3	9968.4
PE_{total}	kWh d^{-1}	2198.4	2682.0	2428.2	1092.3	1238.8	1188.0
PE_{sludge}	kWh d^{-1}	829.18	882.42	864.98	902.14	945.00	943.63
PE_{permeate}	kWh d^{-1}	1369.2	1799.5	1563.2	190.16	293.80	244.35
PE_{q_w}	kWh d^{-1}	Not recorded	Not recorded	Not recorded	8.00	8.00	8.00
$PE_{q_{int}}$	kWh d^{-1}	Not recorded	Not recorded	Not recorded	480.53	523.39	522.02
PE_{q_r}	kWh d^{-1}	Not recorded	Not recorded	Not recorded	413.61	413.61	413.61
$PE_{q_{eff}}$	kWh d^{-1}	Not recorded	Not recorded	Not recorded	147.77	251.31	201.91
$PE_{q_{back}}$	kWh d^{-1}	Not recorded	Not recorded	Not recorded	42.39	42.49	42.44
ME	kWh d^{-1}	576	576	576	714.38	714.38	714.38
OCI	–	22160.0	23673.3	23851.3	20479.6	20199.6	20656.3
Total SRT	d	27.44	26.04	26.91	33.80	31.90	33.11
Aerobic SRT	d	18.85	18.17	18.56	20.41	19.67	20.10
Y_{obs}	–	0.706	0.743	0.732	0.566	0.599	0.587
FI_i	m^{-1} L^{-1}				4530.2	6282.8	6446.7
FI_r	m^{-1} L^{-1}				71639.6	54281.4	64244.2

Table 15: Comparison of energy costs between IBMF-MBR, BSM-MBR and three full-scale municipal MBR WWTPs - modified from Maere et al. (2011) - Reprinted from Janus and Ulanicki (2014).

Energy cost ($kWh\ m^{-3}$)	Schilde [1)]	Varsseveld [2)]	Nordkanal [3)]	BSM-MBR	IBMF-MBR	
					Open-loop [*)]	Closed-loop [*)]
ME	0.05	0.04	0.11	0.03	0.039	0.039
PE_{sludge}	0.10	0.11	0.01	0.05	0.046	0.049
$PE_{effluent}$	0.07	0.12	0.02	0.07	0.008	0.008
$AE_{bioreactor}$	0.07	0.24	0.11	0.21	0.22	0.22
$AE_{membrane}$	0.23	0.34	0.45	0.53	0.49	0.30
Total	0.52	0.85	0.71	0.90	0.81	0.62

[*)] dry-weather conditions with average permeate flow rate $q_{perm,ave} = 18286.3\ m^3\ d^{-1}$

[1)] Fenu et al. (2010)

[2)] Wever et al. (2009)

[3)] Brepols et al. (2010)

6. Conclusion

In summary, IBMF-MBR was found to be in a good agreement with the ASM1-based BSM-MBR benchmark model whilst additionally providing information on biopolymer production and membrane fouling. Although the simulations showed a few discrepancies between both models with regards to some biological constituents and process parameters, these differences were not significant. IBMF-MBR was found to predict lower denitrification rates compared to BSM-MBR. Although it is impossible at this stage to say if the denitrification rates predicted by IBMF-MBR are closer to the typical values observed on physical systems than those predicted by BSM-MBR, ASM1 was already reported in literature to over-predict denitrification in high SRT systems due to infinite recirculation of biodegradable substrates in the implemented death-regeneration model. IBMF-MBR also predicts lower sludge yields and thus higher SRTs to BSM-MBR due to an altered flow of organic substrates in the biological model caused by the introduction of biopolymer kinetics. Qualitatively, this change is again in a good direction as MBR systems have been reported numerously to produce lower sludge yields to those predicted by standard mathematical models due to large SRTs (Lubello et al., 2009).

The simulations also revealed that irreversible fouling, albeit traditionally predominantly attributed to bulk liquid SMP concentrations, is much more sensitive to flux than SMP. Additionally, under high flow rates across the plant, solids shift downstream from the bioreactor to the membrane tank causing high solids loading on the membrane and thus producing higher reversible fouling simultaneously coinciding with high irreversible fouling. These findings suggest that flow control in MBRs is of an outmost importance. In order to compare the degree of fouling associated with different operating strategies in a MBR benchmark model, two fouling indices, respectively for irreversible and reversible fouling, have been introduced and calculated for each control strategy investigated in this paper. These fouling indices can also be used to calculate fouling cost indices in order to quantify the financial operational costs associated with fouling mitigation.

The simulated bulk liquid SMP and EPS concentrations exhibit rather modest variabilities under all dynamic weather conditions, mainly due to diurnal loading pattern in dry weather and dilution effects in wet weather, while steady-state bulk-liquid SMP and EPS concentrations were earlier found to change noticeably with the operating conditions such as e.g. SRT (Janus and Ulanicki, 2015a). It is possible that the variability of SMP and EPS in physical full scale WWTPs would be higher as the biopolymers were found to be produced predominantly under stress conditions such as toxicity, osmotic shocks, large disturbances in influent flow and loading rates or high shear intensities (Noguera et al., 1994; Barker and Stuckey, 1999; Wingender et al., 1999) while our CES-ASM1 biological model describes the biopolymer kinetics only with a standard Monod equations. Therefore, the contribution of SMP and EPS to irreversible and reversible fouling under dynamic conditions may be underestimated in the model as, first, some biopolymer production dynamics might not have been identified during calibration and, second, the model itself may not describe these dynamics. Lack of validation of standard biopolymer production models in activated sludge systems operating under dynamic conditions is the main bottleneck of the IBMF-MBR model as well as other integrated MBR models, alongside the nature of the functional relationships between biopolymer concentrations and fouling. These topics need to be researched in the future to allow development of more realistic MBR models.

In summary, IBMF-MBR, despite of its shortcomings listed above, offers additional benefits compared to the BSM-MBR model as it additionally allows to quantify the bulk liquid biopolymer concentrations, the rates of fouling and the energy consumption for air-scouring and pumping. These features allow the modeller to benchmark process control schemes while taking into account the effects of fouling on process performance, which is not currently possible with the BSM-MBR benchmark model. They also allow the modeller to build fully functional MBR simulation models which can be used for process design, process optimisation, controller design and testing new plant configurations.

References

Ahmed, Z., Cho, J., Lim, B.R., Song, K.G., Ahn, K.H., 2007. Effects of sludge retention time on membrane fouling and microbial community structure in a membrane bioreactor. Journal of Membrane Science 287, 211–218.

Barker, D.J., Stuckey, D.C., 1999. A review of soluble microbial products (SMP) in wastewater treatment systems. Water Research 33, 3063–3082.

Brepols, C., Schafer, H., Engelhardt, N., 2010. Considerations on the design and financial feasibility of full-scale membrane bioreactors for municipal applications. Water Science and Technology 61, 2461–2468.

Broeckmann, A., Busch, J., Wintgens, T., Marquardt, W., 2006. Modeling of pore blocking and cake layer formation in membrane filtration for wastewater treatment. Desalination 189, 97–109. Selected paper from the 10th Aachen Membrane Colloquium.

Busch, J., Cruse, A., Marquardt, W., 2007. Modeling submerged hollow-fiber membrane filtration for wastewater treatment. Journal of Membrane Science 288, 94 – 111.

Copp, J.B., 2002. The COST simulation benchmark - description and simulator manual. Luxembourg: Office for Official Publicatios of the European Communities. ISBN: 92-894-1658-0.

Di Bella, G., Mannina, G., Viviani, G., 2008. An integrated model for physical-biological wastewater organic removal in a submerged membrane bioreactor: Model development and parameter estimation. Journal of Membrane Science 322, 1–12.

Fenu, A., Roels, J., Wambecq, T., Gussem, K.D., Thoeye, C., Gueldre, G.D., Steene, B.V.D., 2010. Energy audit of a full-scale MBR system. Desalination 1-3, 121–128.

Hoa, P., Nair, L., Visvanathan, C., 2003. The effect of nutrients on extracellular polymeric substance production and its influence on sludge properties. Water SA 29, 437–442.

Janus, T., Ulanicki, B., 2014. Integrated mathematical model of a mbr reactor incuding biopolymer kkinetic and membrane fouling. Procedia Engineering 70, 882–891.

Janus, T., Ulanicki, B., 2015a. ASM1-based Activated Sludge Model with Biopolymer Kinetics for Integrated simulation of Membrane Bioreactors for Wastewater Treatment. Procedia Engineering 119, 1318–1327. Computing and Control for the Water Industry CCWI2015 Sharing the best practice in water management.

Janus, T., Ulanicki, B., 2015b. A Behavioural Membrane Fouling Model for Integrated Simulation of Membrane Bioreactors for Wastewater Treatment. Procedia Engineering 119, 1328–1337. Computing and Control for the Water Industry CCWI2015 Sharing the best practice in water management.

Janus, T., Ulanicki, B., 2015c. Interface Model between the Bioreactor and the Membrane in a Membrane Bioreactor for Wastewater Treatment. Proce 119, 1338–1347. Computing and Control for the Water Industry CCWI2015 Sharing the best practice in water management.

Liang, S., Song, L., Tao, G., Kekre, K.A., Seah, H., 2006. A modeling study of fouling development in membrane bioreactors for wastewater treatment. Water Environment Research 78, 857–863.

Lu, S.G., Imai, T., Ukita, M., Sekine, M., Higuchi, T., Fukagawa, M., 2001. A model for membrane bioreactor process based on the concept of formation and degradation of soluble microbial products. Water Research 35, 2038–2048.

Lubello, C., Caffaz, S., Gori, R., Munz, G., 2009. A modified activated sludge model to estimate solids production at low and high solids retention time. Water Research 43, 4539–4548.

Maere, T., Verrecht, B., Moerenhout, S., Judd, S., Nopens, I., 2011. BSM-MBR: A benchmark simulation model to compare control and operational strategies for membrane bioreactors. Water Research 45, 2181–2190.

Nagaoka, H., Yamanishi, S., Miya, A., 1998. Modeling of biofouling by extracellular polymers in a membrane separation activated sludge system. Water Science and Technology 38, 497–504.

Noguera, D., Araki, N., Rittmann, B., 1994. Soluble microbial products (SMP) in anaerobic chemostats. Biotechnology & Bioengineering 44, 1040–7.

Nuengjamnong, C., 2006. The investigation of soluble microbial products in membrane fouling. Thai Journal of Veterinary Medicine 36, 31–38.

Wang, Z., Wu, Z., Tang, S., 2009. Extracellular polymeric substances (EPS) properties and their effects on membrane fouling in a submerged membrane bioreactor. Water Research 43, 2504–2512.

Wever, H.D., Brepols, C., Lesjean, B., 2009. Decision tree for full-scale submerged MBR configurations. Final MBR-Network Workshop, 31 March - 1 April, Berlin Germany .

Wingender, J., Neu, T.R., Flemming, H.C., 1999. Microbial Extracellular Polymeric Substances: Characterization, Structures and Function. Springer-Verlag, Berlin, Heidelberg.

Zaisha, M., Dukler, A.E., 1993. Improved hydrodynamic model of two-phase slug flow in vertical tubes. Chinese Journal of Chemical Engineering 1, 18–29.

Zarragoitia-González, A., Schetrite, S., Alliet, M., ad Claire Albasi, U.J.H., 2008. Modelling of submerged membrane bioreactor: Conceptual study about link between activated sludge biokinetics, aeration and fouling process. Journal of Membrane Science 325, 612–624.